CHAPTER

9

River flow monitoring with unmanned aerial system

Dariia Strelnikova[1], *Matthew T. Perks*[2], *Silvano F. Dal Sasso*[3] *and Alonso Pizarro*[4]

[1]School of Geoinformation, Carinthia University of Applied Sciences, Villach, Austria [2]School of Geography, Politics and Sociology, Newcastle University, Newcastle upon Tyne, United Kingdom [3]Department of European and Mediterranean Cultures: Architecture, Environment and Cultural Heritage (DICEM), University of Basilicata, Matera, Italy [4]Department of Civil Engineering, Diego Portales University, Santiago, Chile

9.1 Introduction

Streams and rivers throughout landscapes, similar to arteries and veins in a body, pump priceless lifeblood, without which our planet and life itself are unimaginable—fresh water. Diverse applications stimulate the demand for fresh water: public supply and hydropower, commercial and industrial use, domestic needs, irrigation, and livestock production (Gleick, 2003; Renzetti, 2002; Schoengold and Zilberman, 2007). Monitoring streams and rivers are performed for practical reasons, research purposes, and environmental concerns. Practical applications may be focused on supporting commercial projects, such as discharge monitoring at a hydropower dam or turbidity analysis during dredging. Research applications often deal with studying aspects of watercourse hydrology. Monitoring of running waters for environmental purposes may target a better understanding of human impact on the ecosystem under study and may evaluate the effects of protection and restoration measures in the area of interest.

Fresh water is found not only in streams and rivers but also in wetlands, reservoirs, ponds, lakes, and glaciers. However, only streams and rivers are characterized by streamflow—water movement, which profoundly impacts both water quality and the hydrology of watercourses (Zeiringer et al., 2018). Flow observation and measurement are important for disaster prevention and policymaking. Flow monitoring data are necessary for proper water allocation for domestic, industrial, and agricultural uses (Goes et al., 2021). They are crucial for the construction of bridges, for example, due to the necessity to consider the

DOI: https://doi.org/10.1016/B978-0-323-85283-8.00012-6

changes in the river channel size over time (Setiati, 2019). Flow monitoring helps to predict and measure the extent of natural hazards, such as flood (Kiedrzyńska et al., 2015), drought, or landslides, and to plan long-term and immediate measures to reduce the associated risks and harm. It helps identify and maintain the volume of water necessary to preserve river health and its suitability as a habitat for riverine species (Acreman and Dunbar, 2004). An overview of important reasons for flow monitoring is given in Fig. 9.1.

Due to the importance of flow monitoring, various methods and tools have been developed to perform flow observation and measurement correctly, efficiently, and accounting for the peculiarities of each type of watercourses. The major variables influencing the methodology of flow monitoring are width, depth, and slope of the watercourse, the roughness of bed and bank materials, load and size of sediments, flow velocity, and discharge (Dobriyal et al., 2017; John, 1978), as well as the target degree of accuracy and financial limitations. Flow monitoring methods can be subdivided into the following major categories:

1. *direct measurement*, for example, a volumetric streamflow method, or water level measurement and the use of previously developed rating curves;
2. *constricted flow methods*, such as flume or weir methods;
3. *velocity-area methods*, which can be as simple as float and colored dye tracing methods, or involve the application of expert knowledge and professional equipment, such as measurement with the help of propeller current meters or an acoustic Doppler current profiler, radar surface velocity measurements, electromagnetic measurements, and dilution gauging; and

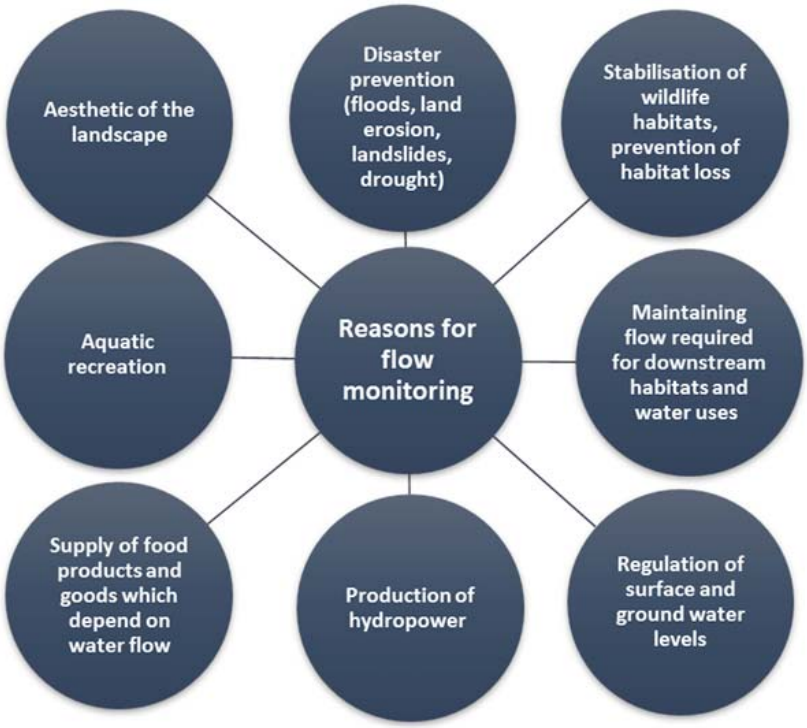

FIGURE 9.1 Reasons for flow monitoring.

4. *image velocimetry* methods.

Since river flow monitoring with the help of unmanned aerial system (UAS) is mostly accompanied by the application of image velocimetry methods, further discussion focuses on the aspects of image velocimetry that is performed with the use of UAS-based optical data. A short summary of other flow monitoring methods is given in Appendix A.

The most popular image velocimetry methods applied for field studies are particle image velocimetry, or PIV (Fujita et al., 1998); space-time image velocimetry, or STIV (Fujita et al., 2007); particle tracking velocimetry, PTV (Brevis et al., 2011; Dal Sasso et al., 2018); Kanade–Lucas–Tomasi image velocimetry, KLT-IV (Perks et al., 2016); optical tracking velocimetry, OTV (Tauro et al., 2018); and surface structure image velocimetry or SSIV (Leitão et al., 2018), with PIV and PTV being the most widely used. The goal of image velocimetry is the measurement of flow velocities based on the analysis of the behavior of traceable features in a time series of optical data depicting streamflow. Examples of optical data suitable for image velocimetry analysis include true-color or grayscale video recordings and sequences of RGB or thermal images. When image sequences are captured with the purpose of image velocimetry, a timestamp of sufficient temporal resolution must be uniquely identified for each image in the sequence; ideally, images should be captured with a constant time delay between them.

In contrast to the flow monitoring methods described in Appendix A, image velocimetry techniques allow to identify surface flow velocities in multiple locations of the captured water surface simultaneously (Detert, 2021). Their application produces instantaneous surface velocity fields (SVFs)—sets of vectors that describe surface velocity magnitude and direction in the locations of single traceable features or in the cell centers of an imaginary grid placed over the captured area. Thus image velocimetry methods allow to not only calculate average flow velocities and discharge but to identify complex flow patterns, which can be of importance for environmental applications (Strelnikova et al., 2020).

In recent years, UAS are increasingly becoming the tool of choice for optical data acquisition with the purpose of image velocimetry (Detert et al., 2017; Koutalakis et al., 2019; Tauro et al., 2016). UAS-based data capture has several advantages over handheld, mobile, or stationary cameras mounted on river banks, bridges, telescopic masts, and angled toward the water surface. It enables the free choice of a study area (Detert et al., 2017), independent of structures suitable for camera mounting and accessibility of watercourse banks. Optical data can be captured with the help of UAS in unfavorable flow conditions, for example, during floods (Perks et al., 2016). The possibility to capture data at nadir from comparatively high flight heights (i.e., distance measured from the local surface) enables data acquisition at wide rivers without the loss of data quality, which is observed toward the remote river bank when optical data are captured from the opposite bank at an oblique camera angle (Strelnikova et al., 2020). The flexibility of flight height selection provides more options in terms of spatial resolution of captured data. Optical data recorded at a nadir position, in many cases, require no orthorectification (Tauro et al., 2014a). All these factors, together with the improvement of built-in sensor quality and decreasing UAS acquisition costs, lead to the increasing popularity of streamflow monitoring with the help of UAS.

9.2 General workflow of river flow monitoring with UAS

River flow monitoring with the help of UAS and image velocimetry methods includes the following steps:

1. data acquisition
2. data preprocessing
3. data processing
4. data postprocessing

At the stage of data acquisition, it is necessary to select the extent of the study area, the target spatial and temporal data resolution, the optimal wavelength range (visible light, infrared), and the corresponding camera sensor. Further, a carrier platform must be selected, for example, a multirotor UAS for data acquisition while hovering over a fixed location. The camera angle is selected depending on the size of the study area, study goals (e.g., measuring average flow velocity vs acquiring detailed surface flow patterns), desired spatial resolution of data, and the demands of the selected image velocimetry method. The quality of captured data will depend on weather conditions and illumination and will suffer in strong winds, rain, or abundant sun reflections on the water surface, complicating tracer recognition. To enable image velocimetry, a flow must contain traceable features. If no features suitable for the selected image velocimetry method are present in the flow, they must be introduced into the flow artificially.

The stage of data preprocessing involves masking out irrelevant areas of images to reduce the computational effort. It may include image enhancement to increase the recognizability of traceable features, which is performed by means of consecutive application of various filters. Data preprocessing may also include image stabilization and geometric correction, such as orthorectification or removal of lens distortions.

Data processing is performed with the use of the selected image velocimetry method (PIV, PTV, STIV, KLT-IV, OTV, SSIV, etc.). It involves the calculation of surface velocity vectors based on the magnitude and direction of displacements of traceable features. The displacements are identified by comparing consecutive images or video frames to each other, and the velocities are calculated using the known time delay between the images/video frames.

Spurious vectors and outliers are detected and removed at the data postprocessing stage. Further operations applied to the calculated surface velocity fields at this stage are spatial and temporal interpolation, smoothing, and aggregation. At the end, image velocimetry results are visualized and/or exported in a target exchange format.

9.3 Best practices of data acquisition

9.3.1 General considerations concerning data acquisition

Independent of the purpose of data collection, some important aspects must first be considered when using UAS platforms for data acquisition. First, it is necessary to be informed of the legal aspects of UAS use in the country where the study area is located.

UAS-related regulations in many countries are very dynamic. The knowledge about requirements and restrictions associated with UAS use, such as UAS pilot certification, UAS platform registration, procedures for operation risk assessment, flight height, and altitude limitations or locations of no-fly zones, must be retrieved from official channels and responsible authorities prior to the UAS flight. Independent of the legal requirements, a pilot operating the UAS must be competent and prepared to take proper action in case of emergencies, such as loss of control over the UAS, to minimize the extent of possible harm. Flight planning must be done thoroughly and under consideration of environmental and privacy concerns. An important aspect in UAS-based data capture is the weather: it must be suitable for the operation of the selected UAS platform in terms of its technical limitations (e.g., wind speed), and within the limitations of the method (e.g., favorable light conditions). More detailed guidance with respect to UAS operation planning and safety measures is provided in Chapter 3.

The market of UAS sensors and platforms that can be used for optical data capture is dynamic, featuring new technological advances each year (Jeziorska, 2019). Attempts have been made to create a summary of UAS-based technologies suitable for hydrological applications, including the analysis of downsides and advantages of different UAS platforms and compatible sensors (Jeziorska, 2019). Chapter 2 provides some additional information with regards to this topic.

An important difference between the UAS platforms is their architecture: fixed-wing platforms are characterized by higher endurance but are incapable of hovering and are often associated with higher costs than multirotor UAS. For this reason, data collection with the goal of image velocimetry is mostly performed with the use of multirotor UAS platforms (Cao et al., 2020; Detert et al., 2017; Fujita et al., 2015; Pearce et al., 2020; Strelnikova et al., 2020). RGB videos are the most used types of optical data collected for image velocimetry purposes. The likely reason for it is the fact that many multirotor UASs are equipped with high-resolution built-in RGB cameras capable of video recording, while thermal cameras are more expensive. Also, thermal cameras rely on strong temperature signal, which is not always the case for small rivers. Processing of thermal images is more complicated in comparison with the processing of RGB videos, too, especially due to the absence of dedicated software for image velocimetry with the use of thermal imagery.

9.3.2 Traceable features

Image processing techniques require visible patterns on the water surface to track their movement in time and compute velocities. In some cases, minimal changes in the intensity of the water surface color are identified and taken as tracers. In other cases, natural patterns on the free water surface, like wave crests, vortexes, bubbles, or natural floating material (e.g., debris, vegetation), provide sufficient seeding for image velocimetry processing. In flood flow conditions, surface ripples generated by the effects of near-surface turbulence and pressure fluctuation are often used as natural unseeded tracers. Fujita and Kunita (2011) demonstrated that an oblique-scanning helicopter-mounted camera can identify the water surface's movement by examining water ripples generated by turbulence or differences in color caused by variations in suspended sediment concentration,

without the need for artificial tracers. Dugan et al. (2014) used small-scale temperature variations on the water surface as tracers visible on infrared imaging.

In the absence of natural features (generally in low flow conditions), artificial tracers (seeding) have to be added to the flow to improve the performance of velocimetry analysis. The choice of particles for tracing in field conditions is different from laboratory experiments where illumination and flow regime can be controlled. According to Detert and Weitbrecht (2015), particles used as tracers "should have a sufficient floating behaviour, significant colour contrast, a passive response to the flow, the possibility of a simple mass production at adequate dimensions, and no effect on the water quality." Floating particles should have sufficient contrast against the water surface to be visible at the desired platform height (usually 10−100 m) and remain visible in the presence of environmental noise (illumination conditions and water reflections). Image velocimetry techniques are indirect as they determine the velocity of tracer particles rather than the velocity of the fluid that carries them. Thus tracers must have a weight density (e.g., g/cm^3) similar to water: low-density tracers tend to be nonsubmerged for most of their volume and thus be significantly affected by wind, and high-density tracers tend to be nearly fully submerged and therefore not properly visible.

Based on these requirements, and with respect to ecological concerns, different biodegradable materials have been exploited as tracers in field campaigns: woodchips (Kim et al., 2008), candles (Sukhodolov et al., 2007), rice crackers (Fujita and Hino, 2003), charcoals (Dal Sasso et al., 2018), and ecofoam (Sutarto, 2015). Dal Sasso et al. (2018) used different types of tracers in clear or turbid waters (woodchips and charcoal, respectively) to increase the contrast differences between the traceable features and the background. Strelnikova et al. (2020) proposed the use of ecofoam tracers colored with environment-friendly dyes. Tauro et al. (2012) used bee wax-based fluorescent particles tracers for experimental measurements in small-scale streams to overcome the problems related to illumination conditions and particle visibility. Furthermore, Tauro and Grimaldi (2017) proposed a combination of ice tracers and a thermal camera to characterize surface flow velocities with the PTV algorithm. The typical weight density of tracers is less than 1 g/cm^3, for example, literature values for charcoal and woodchip tracers are 0.208 and 0.380 g/cm^3, respectively.

Tracers are almost irregularly shaped because of their natural characteristics and material involved (squared, spherical, or cylindrical). The average dimension is typically of few centimetres (2−8 cm) and the thickness of a few mm (2−4 mm). Ecofoam is usually cylindrical and thicker, around 1.5 cm in diameter.

In most cases, artificial tracers are manually deployed on the free water surface by operators located upstream of the cross-section monitored: on the bank, on the bridge, or in a boat. During the distribution of the tracers, it is necessary to release the particles from different locations to cover the entire cross-section width (Strelnikova et al., 2020). It is recommended to introduce tracers into the flow outside of the UAV field of view (FOV) to allow them to adjust to the flow before they start being traced. In the case of a large river, homogeneous distribution of tracers in the area of interest usually requires a large number of artificial tracers and multiple people for tracer deployment (Pearce et al., 2020; Strelnikova et al., 2020). Tracers are expected to accurately follow the underlying flow and be uniformly distributed in the area to be measured, reducing the possibility of self-agglomeration and inhomogeneous distribution across the area of interest.

Seeding density and spatial distribution of tracers are among the most critical factors for successfully applying image velocimetry techniques (Raffel et al., 2018). Seeding density (also called seeding concentration) represents the number of particles transiting on the water surface during field surveys and generally is expressed as particles per pixel (ppp). For most image velocimetry techniques, low seeding densities are associated with larger errors. In contrast, a sufficiently high seeding density ensures optimal conditions for tracking algorithms and consequently reduces the uncertainty and errors in velocity estimations. The entity of the errors is variable and depends on the sensibility of the technique to this parameter (Dal Sasso et al., 2020). The spatial distribution of tracers indicates whether tracer patterns are uniformly or randomly distributed in space. This factor varies significantly during the recording period. This variability depends on different aspects: the hydrodynamic characteristic of the flow, the morphological characteristics of the river reach, the type and amount of material deployed, and the number and experience of operators deploying the tracers. Of further consideration is that the actual seeding density (i.e., observed by an operator in the field) is likely to be higher than the effective seeding density (i.e., observed by the tracking algorithm) due to difficulties encountered by features detection algorithms in correctly identifying all tracers (Dal Sasso et al., 2020).

9.3.3 Reasons to use ground control points

After optical data acquisition, it is necessary to (1) remove instability and distortions and (2) geo-reference the acquired data or at least identify the relation between the image units and the real-world units for the purpose of calculation of flow velocities in m/s as opposed to pixel per frame. The aforementioned transformations can be done when captured optical data contain easily identifiable motionless features with known coordinates or known distances between them. To guarantee that such motionless features are present in the FOV and that their coordinates or distances between positions are measured correctly, it is a common practice to use ground control points, or GCPs (also called ground reference points). The GCP markers are placed in the FOV in a controlled manner as close to the water surface as possible (Detert et al., 2017; Le Coz et al., 2010). Their coordinates are usually determined with the help of a differential global navigation satellite system, including differential global positioning system, or D-GPS (Strelnikova et al., 2020) or a total station (Le Coz et al., 2010), but low-cost GPS devices can be used for this purpose as well (Detert et al., 2017). When the river or stream under study is narrow and the distances between the GCPs are short, it is preferable to perform accurate measurements of distances between the GCPs using a measuring tape rather than a low-cost GPS device. In this case, it is important to make sure that GCPs are coplanar to the water surface. Considering one of the GCPs as the origin, it is possible to calculate the relative coordinates of the other GCPs and use them for image distortion removal and scaling. More information about the minimum number of GCPs, their optimal placement, and the best patterns of GCP markers is provided in Chapter 8.

In the absence of GCPs or other features with known coordinates, there exist other approaches to calculating the ratio between the image units and the real-world units. If at least one object of known and sufficiently large dimensions is present in the FOV during

data acquisition or if distances between some of the objects are known, these data can be used for image calibration. If no such objects naturally occur, they may be introduced into the FOV. For example, Tauro et al. (2014b) suggested using a system of lasers to project points onto the water surface at a known distance from each other for further image calibration. The approaches mentioned earlier, however, work only if captured data are free from lens distortions and have a uniform scale (capture at nadir, flat terrain).

9.3.4 Flight height

The selection of the flight height for data acquisition should be done based on the following considerations:

1. the extent of the study area (target size of the FOV),
2. the pixel resolution of the available sensor,
3. target ground sampling distance (for the tracers to be visible),
4. the level of detail of the target SVF (minimum size of flow structures that must be recognized),
5. obstacles interfering with the signal or shading the FOV,
6. legal limitations, and
7. battery life of the UAS and other technical limitations.

The extent of the study area and technical characteristics of the selected camera sensor influence the minimum flight height at which the entire extent of the study area falls within the FOV. Additional to the water surface, the study area should include river banks with motionless features, which can be used for image stabilization and removal of various distortions. This requirement holds even if there are well-distributed motionless features in the middle of the river.

The size of tracers is an important criterion that influences the recognizability of individual traceable features in the acquired optical data depending on their spatial resolution. It may represent a limitation that prevents capturing the entire width of a large river: in case of higher flight height that would increase the FOV to the target extent, image resolution may be reduced such that tracers will not be recognizable. Possible solutions, in this case, include (1) reduction of the extent of the FOV by subdividing the study area into subareas, each of which has to include motionless features necessary for image preprocessing; (2) replacing the selected camera sensor with one that has a better resolution; or (3) selection of larger tracers. Some tracers, like ecofoam, tend to form clusters that are easy to recognize from high flight heights (Strelnikova et al., 2020). However, it is important to keep in mind that an increase in the size of traceable features means a simultaneous reduction of the spatial resolution of the resulting SVF. Thus, with the increase in flight height, flow structures of small size are likely to become unrecognizable (Lewis and Rhoads, 2018).

Another important factor to consider when selecting flight height is obstacles. In some areas, the peculiarities of the terrain and vegetation may influence the quality of the GPS signal or the link quality between the UAS and the ground station. Further, high obstacles such as power lines may not only cause link disturbance but also obscure the FOV.

As mentioned earlier, it is important to ensure that legal conditions that allow UAS operation at a desired height are met. Operational limitations of the UAS, such as battery life, must also be considered: reaching a higher height requires time, which reduces the maximum duration of video recording. It is necessary to make sure that the battery is fully charged, especially when operating UAS at low air temperatures.

Since winds tend to be stronger at higher flight heights, it is crucial to avoid high-height flights when wind conditions near the Earth's surface are close to the operational limits of the selected UAS platform. UAS operation at high heights also leads to the increase of the magnitude of camera movement in ground distance (Lewis and Rhoads, 2018), such that even subpixel apparent motion may introduce errors in flow velocity calculation.

9.3.5 Duration of the video for image velocimetry analysis

Several factors influence the optimal duration of video recording with the purpose of image velocimetry. The video should be long enough to ensure that the tracers achieve the best possible distribution across the study area and fully advect across the FOV. Ideally, it would be possible to split the video into several chunks which would be analyzed separately to determine the uncertainty in SVFs. On the other hand, long videos pose challenges:

- Long videos are often characterized by a higher amount of camera movement, as well as changing light conditions.
- Maintaining sufficient seeding density and proper distribution of artificial tracers for a prolonged period of time is challenging and associated with high costs.
- The size of available data storage may also present a limitation when dealing with high-resolution videos and imagery. For example, the maximum video size for popular DJI drones is 4GB which is equivalent to $<$7-min of video acquisition at 2720×1530 px.
- Analysis of long videos increases the computational effort required, especially for frame rates exceeding 25 fps.

Thus it is a common practice to record relatively short videos, around 5 min in length, and then to perform image velocimetry using video portions (see Section 9.9) of about 30 s in length (Lewis and Rhoads, 2018; Pearce et al., 2020; Strelnikova et al., 2020). Some studies exploit longer videos or image sequences, up to 1–3 min (Cao et al., 2020; Detert et al., 2017). It must be kept in mind that if the videos used for image velocimetry are too short, macro-turbulences are not sufficiently captured and thus cannot be reflected in the velocimetry results.

9.3.6 Metadata

Accurate recording of metadata at the stage of data acquisition plays an important role at later stages of data analysis. These metadata include:

1. location and extent of the study area,
2. date and time of data capture,

3. duration of recording,
4. UAS platform and sensor characteristics,
5. flight height,
6. GCP coordinates or distances between GCPs,
7. weather conditions,
8. reference measurements (flow velocity in selected locations, discharge),
9. characteristics of the tracers used, and
10. other information relevant for a particular study, for example, water temperature and water level.

An example of a data acquisition log is given in the Appendix B. Further considerations regarding metadata, which should be recorded at the stage of UAS-based data collection, are discussed in Chapter 3.

9.4 Data preprocessing

Videos adopted for image velocimetry applications should be properly preprocessed based on the environmental and flow charactistics (see Table 9.1).

9.4.1 Sampling image frequency and resolution

Image velocimetry techniques estimate velocities by dividing the displacement of particles between consecutive frames by the time interval between the pair of images. For this reason, spatial and temporal resolutions of the acquisition play a key role and depend on the local flow velocities and physical pixel size. The camera frame rate (that controls the particle displacement between two consecutive images) must be identified properly to avoid over- or undersampling that may lead to errors. Brevis et al. (2011) show that frame-by-frame particles displacements should be larger than tracer dimensions to allow motion tracking. This suggests an operative criterion for choosing a frame rate proportional to the local flow velocity to be set (e.g., from 24 to 60 fps), subsampling it for slow flows to reduce computational loads.

9.4.2 Image stabilization, geo-referencing, and correction of geometric distortions

Optical data captured with the help of UAS may contain various distortions or depict apparent movement of motionless features due to instability of the UAS platform. In the case of applying image velocimetry to a video or image sequence that contains lens or perspective distortions or is unstabilized, data processing yields erroneous results (Detert and Weitbrecht, 2015). Image stabilization is used to remove the effects of camera vibration and movement, which take place during data capture. Geometrical corrections are performed to remove perspective distortions, which may be observed in the case of oblique camera angles or elevation variability within the FOV, and lens distortions. In addition to geometric corrections, a complete geo-referencing may be performed to identify the correspondence between the image space and the real-world coordinates of the study area.

Orthorectification of the acquired footage may be necessary even in cases when it has no visible scale differences which could be attributed to a perspective distortion. In practice, even when an orthogonal camera angle has been targeted during the data acquisition, slight differences from nadir (1−5 degrees) can be observed in the resulting imagery (see Section 9.9). Since even a 2-degree difference from nadir is known to bias image velocimetry results in case of lacking image orthorectification (Detert, 2021), it is important to evaluate the actual camera angle from the acquired footage and to perform orthorectification if differences from nadir are observed. If an orthorectification step is skipped, the velocimetry results in pixels/frame shall be converted into real-world units by means of intersecting the start and end points of each identified feature trajectory with the water surface, calculating the distance between these points, and then calculating the velocity of feature displacement using the known frame rate (Eltner et al., 2020).

Geometric transformations that are performed to remove geometric distortions and/or to stabilize the images may attribute to the uncertainty of flow velocity measurements by reducing image sharpness. This uncertainty is most significant in cases when the displacement of traceable features between the frames lies in the subpixel range.

Depending on the distribution of motionless features, their elevation in comparison to the water surface, consistency of their presence within the FOV, and on the type of geometric transformation applied, some regions of a transformed image may experience more distortion than others. This is especially the case if these regions are located outside the convex hull formed by the motionless features. Thus it is advisable to perform image stabilization and geometric correction using motionless features that are present in all of the processed frames, across the FOV, and at the same elevation as the water surface. More information about the best practices in image stabilization and correction of geometric distortions can be found in Chapter 9.

9.4.3 Image enhancement

Optimizing data capture conditions and image stabilization are not the only ways to increase the quality of image velocimetry results. In most cases, an application of image preprocessing techniques helps to increase the visibility of traceable features and thus to avoid or reduce typical image velocimetry errors such as false correlation caused by background noise. A large group of data preprocessing techniques that can improve the accuracy of image velocimetry analysis are filtering techniques.

One of the such techniques is an *intensity high-pass* filter, which copes with the consequences of inhomogeneous illumination and emphasizes individual particles by suppressing low-frequency information (Thielicke and Stamhuis, 2014). This creates a more homogeneous background, as can be seen in Fig. 9.2B. *Wiener* filter that employs a spatially adaptive statistical model is a popular and well-performing solution for image noise reduction (Kazubek, 2003). It is especially useful when traceable features are relatively large when compared to the frequency of background noise. An example of background noise smoothing by means of the Wiener filter is given in Fig. 9.2C. Wiener filter is often applied after the high-pass filter, which allows to successfully remove the residual noise (Fig. 9.2D).

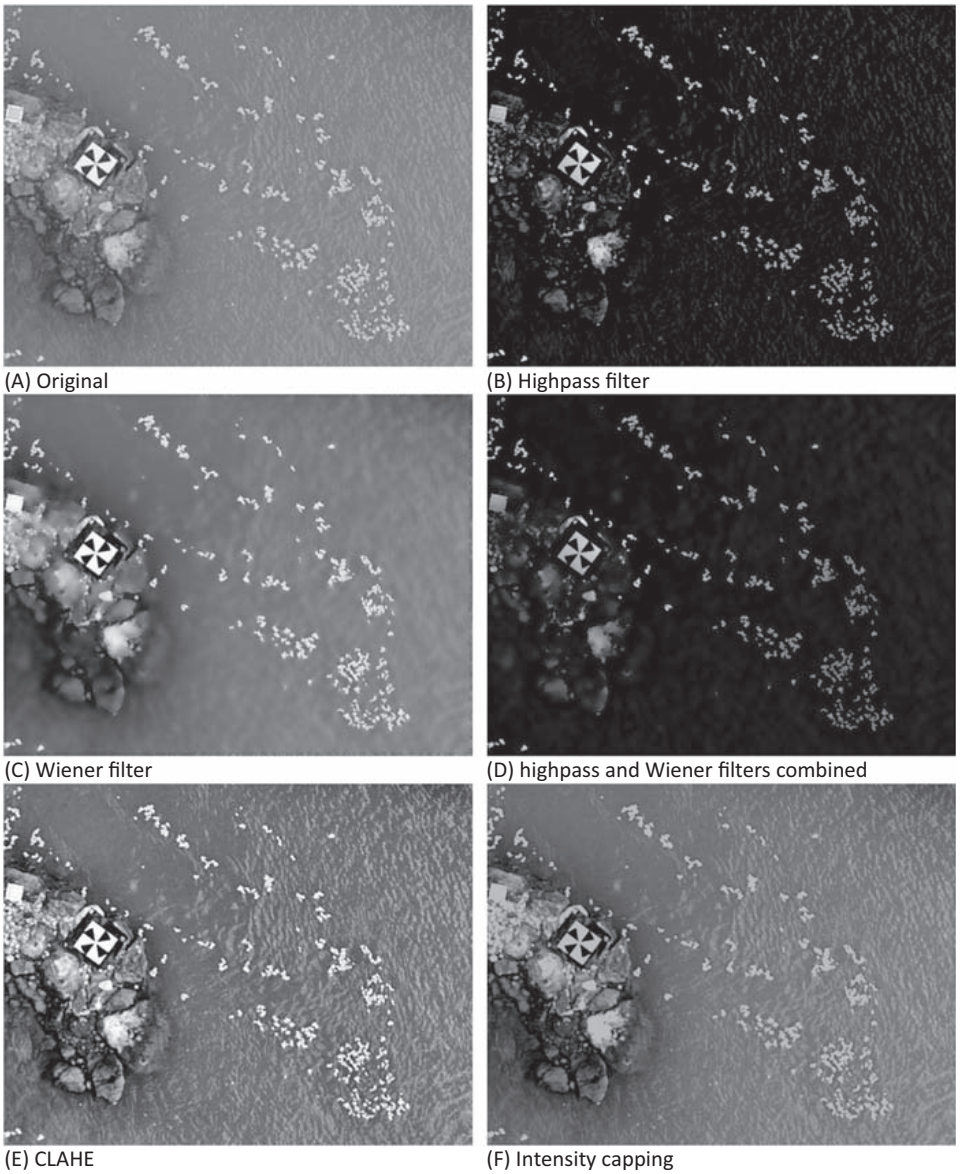

FIGURE 9.2 Application of different image enhancement filters to the footage captured at the Drava River (Austria) in 2020. (A) Original, (B) high-pass filter, (C) Wiener filter, (D) high-pass and Wiener filters combined, (E) CLAHE, and (F) intensity capping. *CLAHE*, Contrast limited adaptive histogram equalization.

Another commonly used image enhancement technique is the *contrast limited adaptive histogram equalization*, or *CLAHE* (Pizer et al., 1987). CLAHE improves the contrast in an image by redistributing the lightness value based on histograms computed from the image parts. It increases the visibility of artificial tracers and wave patterns in turbid water (Fig. 9.2E). However, if the water is clear and the river bed is visible, the application of CLAHE increases the noise and reduces tracer visibility (Fig. 9.3).

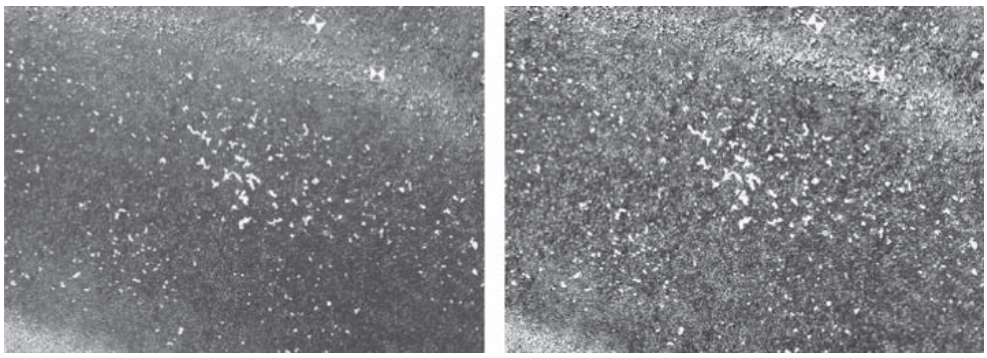

FIGURE 9.3 Application of CLAHE to an UAS-based photograph of a river with a visible rocky bed. (A) Original and (B) filtered with CLAHE. *CLAHE*, Contrast limited adaptive histogram equalization.

Image preprocessing may also include an application of the *intensity capping* (Fig. 9.2F). Intensity capping deals with bright spots in the image, which may bias the velocity vectors. It is based on defining the upper limit to the grayscale intensity of the images and replacing all the exceeding intensity values with this upper limit (Shavit et al., 2007). The main difference to CLAHE is that intensity capping affects only the high-intensity pixel values, while CLAHE causes global modifications.

One more image enhancement technique, the background subtraction, may be particularly useful in clear water conditions with visible river bed or in cases when misleading standing waves interfere with flow pattern calculation. It is possible to use an existing background image without tracers or calculate a background image based on an image sequence with tracers. Fig. 9.4 shows 3 input images (A-1, A-2, and A-3) out of a series of 98 images, a median background image calculated based on the whole sequence and the result of the subtraction of this background image from the image A-1.

9.4.4 Quantification of seeding characteristics

The quantification of spatial and temporal characteristics of seeding during the video acquisition period represents an important task to maximize image velocimetry performances. Dal Sasso et al. (2020) and Pizarro et al. (2020b) introduce three metrics based on the calculation of the (1) seeding density, (2) index of dispersion of tracers, and (3) coefficient of variation of tracer dimension demonstrating their statistical significance on image-based performances and releasing the developed codes. Seeding density, expressed as particles per pixel, is quantified through an automated process that detects and describes features (local corners, blobs, or regions of uniform intensity) inside the region of interest (ROI) during the frame footage. The aggregation level is quantified through the dispersion index D and is a measure of spatial clustering or dispersion of seeding. $D = \sigma^2/\mu$, where σ^2 and μ are the variance and mean values of the seeding density computed in subpatches of the same size. This metric is normally measured to quantify whether a set of events are clustered or dispersed. As in the numerical case, $D = 1$ means features follow a Poisson distribution, while $D < 1$ and $D > 1$ follow an over- and

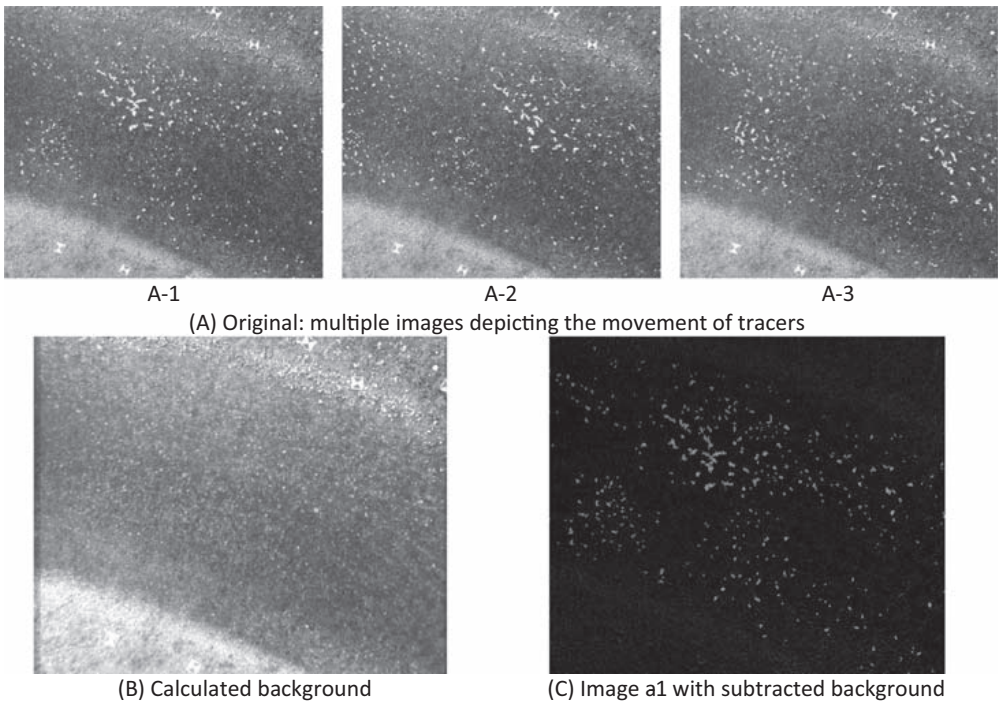

FIGURE 9.4 Background calculation and subtraction. (A) Original: multiple images depicting the movement of tracers, (B) calculated background, and (C) image A-1 with subtracted background.

underdispersed spatial distribution. Finally, the dimension of tracers and their homogeneity is quantified using the coefficient of variation of tracer areas (CVArea).

9.4.5 Selection of the optimal footage portion to analyze

Increasing the duration of the processed video sequence represents an important issue for the performance increment of the techniques. A systematic reduction of errors is observed in numerical experiments (Manfreda et al., 2019; Pumo et al., 2021) and laboratory flumes (Samarage et al., 2012) by increasing the number of frames. This evidence is due to the fact that a higher number of frames increases the number of velocity samples in space and can help to smooth out outliers and noise with a consequent reduction of errors. This effect is particularly evident for low seeding conditions and where particles are not uniformly distributed over the entire frame sequences. However, this beneficial effect is not always observed in natural environments, where considering a large number of frames leads to increasing the occurrences of possible environmental disturbances over the video sequence (e.g., camera movements, environmental noise). Moreover, intense computational time and powerful hardware resources are needed to analyze and store long video time series. To solve this issue, Pizarro et al. (2020b) and Pizarro et al. (2020a) recently proposed the Seeding Distribution Index as a

parameter that synthesizes the seeding conditions in the field, merging seeding and spatial distribution characteristics. This dimensionless index was formulated using numerical experiments and tested in some field case studies for describing the heterogeneous spatial distribution of tracers and the tendency to form clusters. Authors show a significant reduction of errors (over 50%) using the criteria proposed instead of using the total number of frames available.

9.4.6 Practical recommendations for data acquisition

1. Be sure you know the legal requirements in the study area and comply with them.
2. Avoid irregular light conditions (e.g., on a sunny day with fast-moving individual clouds) and shadows on the water surface.
3. Avoid strong winds, and remember that winds are stronger at higher heights.
4. The flow must be visually identifiable in the captured footage both qualitatively (structure, direction) and quantitatively (low, high). For this, some natural or artificially added traceable features must be present in the water.
5. If particle tracers (natural or artificial) are used, and the water is clear, make sure that tracers do not get confused with the elements of the river bed. You may need to try different tracer colors before selecting the one that provides the best contrast.
6. If particle tracers (natural or artificial) are used, and the water is turbid, nadir footage is preferable since it requires fewer geometric corrections.
7. Traceable features must be clearly visible in the footage. Therefore particle tracers must have the size of least 1 pixel, but larger tracers are preferable (ideally 5 pixels and more) since they are more likely to not be confused with the background noise.
8. If waves are used as traceable features, oblique angle footage may be preferred over nadir footage. It should be kept in mind that waves may be misleading since their behavior may differ from the actual flow, and as such their use as traceable features requires careful consideration.
9. To enable subsequent geometric correction and stabilization of the captured videos, make sure to have motionless features in the FOV. If data are captured at angles different from nadir, use motionless features with known coordinates or known distances between them to later be able to remove perspective distortions. Use GCP markers when possible. They will also simplify the stabilization of shaky videos.
10. For high flows, make sure to record optical data at a high frame rate (24 fps and more).
11. High frame rate is also preferable for low flight heights.
12. Select optimal portions of the footage before data analysis, try to keep them relatively short (30 s to no more than 3 min) to speed up data processing and avoid the necessity to manage very large data volumes.
13. Carefully record all relevant metadata, especially if you intend to publish your research. It may be impossible to remember important details necessary for data analysis even a short time after the data acquisition. If you repeat experiments often, develop and follow a standard workflow—this will simplify flow measurements and contribute to higher comparability of individual measurements.

9.4.7 Practical recommendations with respect to image preprocessing

Flow characteristics and image quality play essential role in determining which kind of image preprocessing is likely to improve image velocimetry results. A summary of recommended image preprocessing steps suitable for different image and flow characteristics is given in Table 9.1.

TABLE 9.1 Recommended image preprocessing steps.

Image and flow characteristics	Peculiarities of preprocessing
High flow	High flows must be captured with high frame frequency, starting with at least 24 fps.
Low flow, high frame rate	Subsample frames such that the displacements of traceable features between the resulting frames is easy to visually recognize. Ideally, this displacement should be at least 1 pixel per frame for most of the features.
Inhomogeneous flow	In the case of resampling, it is important to make sure that faster moving tracers in the resulting frame sequence can be visually followed, even if it means that slower moving feature displacements lie in a subpixel range.
Shaky image sequences and videos	Perform stabilization. Since it requires image transformation, make sure that other image preprocessing operations that require image transformation are done simultaneously to avoid an accumulation of transformation errors (details in Chapter 8).
Lens distortions	Perform correction with the use of camera calibration values based on a camera model (details in Chapter 8).
Perspective distortions	Perform orthorectification (details in Chapter 8).
Inhomogeneous illumination	Use intensity high-pass filter.
Noise	Apply Wiener filter, high-pass filter.
Low contrast, turbid water	Use contrast limited adaptive histogram equalization (CLAHE). Avoid using it if the river bed is visible.
Bright spots in the image (e.g., sun reflections)	Apply intensity capping, unless tracers and reflections have similar intensity.
Clear water, visible river bed	Try a combination of intensity high-pass filter and Wiener filter. Alternatively, background subtraction can be used.
Long video	Select a portion of the footage from 30 s to 1–2 min in length with the most homogeneous and clearly visible seeding (minimum reflections, minimum changes in illumination). Ideally, this portion should be characterized by maximum stability of the UAS platform (no change in scale and viewing angle, minimum platform displacement, no jitter).

9.5 Data processing

9.5.1 Methods for image velocimetry

The most studied methods used for image velocimetry analysis are PIV and PTV. When applied in the field conditions as opposed to laboratory experiments, they are often referred to as large-scale particle image velocimetry (LSPIV, introduced by Fujita et al. (1998)) and large-scale particle tracking velocimetry (LSPTV, the term first used by Tang et al. (2008)); in many cases though terms PIV/LSPIV and PTV/LSPTV are used interchangeably. Researchers around the world continue working on the improvement of these and the development of new image velocimetry methods, such as the earlier mentioned STIV, KLT-IV, OTV, and SSIV, or the recent Airborne Feature Matching Velocimetry (Cao et al., 2020). A short summary of some established image velocimetry methods and their advantages is given by Pearce et al. (2020).

Two key factors influencing the choice of the most suitable analysis method include:

- the characteristics of traceable features:
  - the presence of natural tracers, including visible structures on the water surface,
  - the shape of tracers,
  - seeding density,
  - the possibility of using artificial tracers if natural tracers are absent.
- availability of reliable software implementing a method which is selected based on the seeding conditions.

If no software automating image velocimetry with the use of a certain method is available, or if the available software is nonintuitive, difficult to use or its costs exceed the available budget, this image velocimetry method rarely gains popularity. Software development is required before such methods can be applied, given that the algorithm is described in sufficient detail and the person willing to use it has programming skills and/or budget for software development. While this is a valid approach in some cases, those who only start their path toward successful application of image velocimetry are more likely to progress faster and to form a better knowledge base by first applying established and proven image velocimetry tools. Therefore, in this section, we focus on the image velocimetry methods, which are implemented within available and well-supported image velocimetry software (as of 2022), namely, PIV, STIV, PTV, and KLT-IV.

PIV (Raffel et al., 2018) uses cross-correlation applied to pairs of undistorted images, separated by a known time interval. The FOV is divided into a grid with given cell size. Each cell represents an "interrogation area" (IA), for which a tracer pattern is recorded. An area of the consecutive frame within which a search for the tracer pattern similar to the one detected within the IA is performed is called the "search area" (SA). The most likely displacement of visible tracers is determined as the maximum cross-correlation coefficient. Sufficient density of traceable features is required across the entire FOV for accurate surface velocity calculations. The IA and SA sizes need to be defined by the user. In its classic implementation, PIV

has fixed IA and SA sizes. However, in cases when tracer distribution is inhomogeneous, or there is a large variation in properties of different subregions of the velocity field, spatially adaptive PIV should be preferred (Theunissen et al., 2010). PIV can provide complete instantaneous surface flow velocity fields, which can be later used for mean velocity and discharge calculation (Detert et al., 2017). It is the most tested technique and, therefore, there exist a lot of literature describing its use in detail.

As opposed to PIV that analyses the displacements of particle groups, PTV consists of individual particle identification and tracking. When using the popular cross-correlation based PTV algorithm developed by Brevis et al. (2011), the centroids of the detected particles are identified in subsequent images to reconstruct the particle trajectory. To enable accurate centroid identification, the size and shape of the particles must be known (Pearce et al., 2020). Unlike PIV, PTV works well in conditions where surface features are sparse and in unsteady flows.

Though less widely known than PIV and PTV, STIV is a well-established image velocimetry method used for over a decade (Fujita et al., 2007) and being constantly improved (Fujita et al., 2019). STIV captures flow velocities by recording pixel arrays along imaginary "search lines," which are set parallel to the direction of the main flow. A pixel array along a search line is extracted for each frame, and these arrays are stacked to form a single image, in which each pixel row shows brightness distribution along the given search line at a new point in time. The resulting images (one per search line) depict brightness variations in time (y-axis) and space (x-axis) and are therefore called "space-time images" (STIs). Surface flow velocity is calculated using the frame rate and the orientation of brightness displacement measured from the STIs. Velocities calculated in this way are time-averaged. For STIV to work, there must be a variation of brightness or color on the water surface along each search line. A big advantage of STIV is that it requires no tracers except for natural waves or foam. It can cover a large measurement area and has been successfully applied to measure surface velocity on rivers over 100 m in width (Fujita, 2017; Fujita et al., 2007).

KLT-IV (Perks, 2020) uses spatial intensity information to detect and search for the position that yields the best match. As PTV, KLT-IV works well in conditions where surface features are sparse and in unsteady flows. Once images are stabilised, the KLT algorithm is applied to the water surface, and surface features are tracked for the calculation of surface flow velocity. The required parameters include the extraction rate (meaning the duration over which individual trajectories are tracked) and the block size.

9.5.2 Tools for image velocimetry

Among the most established tools for PIV are PIVlab (Thielicke and Stamhuis, 2014) and Fudaa-LSPIV (Le Coz et al., 2014). PIVlab is a MATLAB® app/toolbox. It is available at no additional payment for MATLAB users and is open source. Fudaa-LSPIV is not open-source but it is free to use and does not depend on MATLAB. It has a Java interface which calls FORTRAN executables and can be used with Windows or Linux operation systems.

OpenPTV, a software that arose as a collaborative effort of several research groups, currently mainly targets 3D PTV. Its core, a library of the OpenPTV algorithms called liboptv, is written in C and has Python/Cython bindings. There are two separate user interface packages written in Python 3 that can be used with Python/Cython bindings. The software is free and platform independent. Using a Python version of OpenPTV requires a C compiler installed. Compared to PIVlab, Fudaa-LSPIV, or KLT-IV, OpenPTV is more suitable for users with advanced technical skills and is not optimal for processing the flow footage acquired in field conditions. A more suitable and well-supported tool for UAS-based flow imagery is a newer but actively developed and well-supported FlowVeloTool (Eltner et al., 2020) written in Python, free and open source. In addition to PTV, it has an option of using LSPIV for flow velocity analysis.

KLT-IV software (Perks, 2020) is a free-to-use compiled MATLAB application and as such depends only on the MATLAB runtime, which is available for Windows at no cost. Hydro-STIV (Fujita, 2017) is a licensed software for surface flow velocity calculation using either STIV or PTV. The application of PTV in this software can be performed for a relatively small number of floats that need to be selected manually in the initial video frame. More information about the functions of the tools mentioned earlier can be found in Table 9.2.

9.5.3 Practical recommendations for method and tool selection

Practical recommendations regarding the selection of the most suitable image velocimetry method are given in Table 9.3.

The selection of the tool for image velocimetry analysis in the given study conditions can be performed based on the recommended method (Table 9.3) and the additional tool functionality (Table 9.2).

9.6 Data postprocessing

9.6.1 Outlier detection and filtering

Independent of the chosen image preprocessing techniques, image velocimetry may produce incorrect vectors or outliers. Typically, the magnitude of outliers significantly differs from the magnitudes of surrounding vectors, or their direction is not consistent with the surrounding flow pattern. Often, incorrect vectors are located at the edges of the analyzed region. Outliers can be often identified visually with ease. However, a standard image velocimetry analysis involves calculations based on hundreds of image pairs. In these conditions, automation of outlier detection becomes essential. Popular methods of outlier detection include a Global Mean Test (Westerweel, 1994), a Global Histogram Operator, a Vector Difference Test, a Median Test, a Normalized Median Test, a Minimum Correlation Filter, a Z-Score Test (Raffel et al., 2018), and filtering of trajectory lengths and directions (Tauro et al., 2018). According to Raffel et al. (2018), Vector Difference Test, Median Test, and Normalized Median Test have the highest efficiency in comparison to

TABLE 9.2 Functions of image velocimetry tools.

		Short summary of functions				
Method	**Tool**	**Preprocessing**	**Processing**	**Postprocessing**	**Validation**	**Presentation**
PIV	PIVlab (Thielicke and Stamhuis, 2014)	– Image enhancement (high-pass filter, CLAHE, Wiener filter, intensity capping, contrast stretch, background subtraction) – The image scale can be identified by providing frame rate and a known distance between two objects in one of the frames.	Multipass FFT based PIV and ensemble correlation PIV are used to calculate two-component (u, v) flow velocities and their derivatives: velocity magnitude, vorticity, divergence and others.	– Selection of velocity limits based on (u, v) scatterplot – Standard deviation filter – Local median filter – Manual vector removal – Smoothing – Interpolation of missing vectors – Mean velocity calculation based on selected frames	– Extraction of values from a polyline or an area – Flow data export as ASCII, Tecplot or VTK	– Statistics (histograms) – Scatterplots – Vector velocity field presentation (quiver plot) – Raster velocity field presentation
PIV	Fudaa-LSPIV (Le Coz et al., 2014)	– Image stabilization – Scaling or complete orthorectification	PIV is used to calculate two-component (u, v) flow velocities and velocity magnitudes	– Selection of velocity limits based on the magnitude or (u, v) components – Filtering based on the range of correlation values – Velocity averaging	– Discharge calculation	– Vector velocity field presentation (quiver plot) – Raster velocity field presentation
STIV, PTV	Hydro-STIV (Fujita, 2017)	– Orthorectification (simple perspective transformation) – Full geometric correction based on GCPs and camera parameters – Scaling by specifying pixel scale – Night mode for processing videos shot at night	– STIV calculates time-averaged velocities for a predefined cross-section – PTV, with the use of a small number of floats, calculates the velocity of each float	– Manual correction of orientation in STIs for STIV	– Visual analysis of velocity lists and velocity graphs	– Velocity graph for a cross-section – List of average velocities

PTV	OpenPTV https://www.openptv.net/	– Camera calibration – High-pass filtering	3D PTV	No inbuilt postprocessing, but separate libraries can be connected to enable outlier detection	– Visual validation – Data export	– Trajectory plot – Vector velocity field presentation (quiver plot)
PTV, PIV	FlowVeloTool (Eltner et al., 2020)	– Stabilization – Orthorectification	– PTV (settings include maximum number of features, feature brightness, search radius, sensitivity threshold, number of frames to track for, subsampling of frames for tracking etc.) – LSPIV	– Track filtering – Velocity outlier filtering with the use of the standard deviation filter	– Data export	– Trajectory plot
KLT-IV	KLT-IV (Perks, 2020)	– Orthorectification – Stabilization – Image enhancement (high-pass filter, CLAHE, Wiener filter, intensity capping, contrast stretch, background subtraction)	KLT-IV is used to calculate two-component (u, v) flow velocities, velocity magnitudes and normal velocity	– Selection of velocity limits based on a threshold	– Flow data export as ASCII – Discharge calculation	– Vector velocity field presentation – Plotting the platform movement – Plotting cross-section velocities

GCP, Ground control point; *KLT-IV*, Kanade–Lucas–Tomasi image velocimetry; *PTV*, particle tracking velocimetry; *STIs*, space-time images; *STIV*, space-time image velocimetry.

TABLE 9.3 Recommended methods depending on study conditions.

Conditions	Recommended image velocimetry method	Case studies
Unsteady flow	PTV, KLT-IV	Perks et al. (2016)
Steady flow, homogeneous traceable features	PIV	Muste et al. (2008)
Different currents within one river	Separate the FOV into sections or use a method which enables local adaptation of analysis parameters, e.g., STIV, KLT-IV or spatially adaptive PIV	
Rapidly varied flow	Use a method with adaptive interrogation/search areas, e.g., KLT-IV	Perks et al. (2016)
Irregular sizes and shapes of the particles	PIV, KLT-IV	Perks et al. (2016), Strelnikova et al. (2020)
Clustering of tracers	Avoid PTV KLT-IV, STIV are likely to perform well PIV will perform well unless clusters are sparsely distributed	Daigle et al. (2013), Perks et al. (2016), Strelnikova et al. (2020)
Low density of traceable features	PTV, KLT-IV	Perks et al. (2016), Dal Sasso et al. (2018)
High density of traceable features	PIV, KLT-IV	Detert et al. (2017), Pearce et al. (2020)
No traceable features except for waves, reflections, ripples on the surface	STIV	Fujita et al. (2019)
Foam, turbulent structures	STIV, KLT-IV	Fujita et al. (2019), Fujita (2017), Perks et al. (2016)
High degree of data processing automation desired	PIV, PTV, KLT-IV STIV requires more supervision	Fujita et al. (2019)
Standing waves	STIV preferable, PIV not recommended	Detert and Weitbrecht (2015), Strelnikova et al. (2020)
Reverse flow conditions	PTV preferable, PIV depends on implementation (PIVlab version more suitable)	
Only certain locations within the FOV are of interest, complete velocity field is not required	STIV	Koutalakis et al. (2019)

FOV, Field of view; *KLT-IV*, Kanade–Lucas–Tomasi image velocimetry; *PTV*, particle tracking velocimetry; *STIs*, space-time images; *STIV*, space-time image velocimetry.

other filters. In practice, the selection of outlier detection tool depends to the availability of this tool in the data processing software.

9.6.2 Interpolation, smoothing, and aggregation

To close the gaps in the SVF formed by outlier removal, the identified outliers often have to be replaced by interpolated vectors. Since the probability of finding another outlier in the direct neighborhood of the removed outlier can be described by a binomial distribution (Westerweel, 1994), bilinear interpolation is considered to be the best data replacement approach.

Data reduction simplifies the analysis and presentation of image velocimetry results. Averaging approach, though it is not always applicable, is the most often used data reduction measure. In cases of inhomogeneous flow seeding or flow fluctuations, the sequence of images used for averaging must be carefully selected.

9.6.3 Recommendations with regards to data postprocessing

9.6.3.1 Visualization of velocimetry results and data exchange

After postprocessing is finished, data are represented in a graphic form—statically or dynamically—to simplify its visual analysis. Typical visualization techniques include color coding, with a range of colors corresponding to a velocity range, as well as contour and quiver plotting. Animation of image velocimetry data is used to visualize flow fluctuations. For steady flows, a representation of a static image velocimetry vector field can be combined with the original video to simplify the comparison of image velocimetry results with the optically identifiable flow patterns.

Image velocimetry data can be exported in a selected data exchange format to be used in external information systems for the purpose of validation, comparison of hydraulic modeling. Typical exchange formats include a delimiter-separated ASCII, NetCDF, ParaView Tecplot (.tec), TELEMAC Serafin format (.slf), and OVF See Table 9.4.

TABLE 9.4 Recommended data postprocessing steps.

Conditions	Recommended postprocessing steps
The study targets the analysis of general flow characteristics, main flow direction, discharge	Filtering of trajectory lengths and directions
Uniform flow. Vector magnitudes and/or orientations of some vectors in the resulting vector field are visibly different from the magnitudes/orientations of over 50% of their neighbors. Differences are similar throughout the FOV and can be described by a single threshold.	Vector Difference Test Median Test Global Mean Test
Nonuniform flow. Some vectors differ from the majority of their neighbors. The magnitude of differences varies across the FOV.	Normalized Median Test

FOV, Field of view.

9.7 Validation of image velocimetry results

Image velocimetry results can be validated by comparing them with ground truth data—reference flow measurements performed simultaneously or in close temporal relation to the point of data acquisition. These flow measurements may be available in the form of (1) surface velocities, (2) individual point velocities measured close to the water surface, (3) point velocities measured at various depths and converted into depth-averaged velocities, or (4) in the form of discharge. Direct comparison of image velocimetry results with reference data is possible only if reference data represent surface velocities. In the case of depth-averaged velocities and discharge, these derivatives have to be calculated using SVF information before comparison. In any case, it is important to correctly identify the correspondence between the locations of reference measurements in real-world coordinates and the locations of surface velocity vectors within the image space, which is normally done by geo-referencing of image velocimetry data.

9.7.1 Depth-averaged velocities

Water surface velocities can be used to estimate depth-averaged velocities at each vertical water column. Chiu (1989) proposed a probabilistic formulation—relying on the principle of maximum entropy and dimensionless parameters—to derive one- and two-dimensional velocity distributions in open channels. This approach was afterwards simplified by Moramarco et al. (2004), assuming that the entropy-based velocity distribution can be applied to any vertical and the distribution of maximum velocity across the flow area can follow an elliptical or parabolic shape. From a practitioner perspective, a velocity coefficient is generally adopted, which represents the ratio between the maximum and mean flow velocities. This coefficient is a function of the vertical velocity profile and affected by Froude and Reynolds numbers, flow aspect ratio, micro- and macro-bed roughness, and relative submergence of the large-scale roughness elements. ISO 748:2007 (2007) suggests this coefficient ranges between 0.84 and 0.90, with the highest values usually obtained for smooth river beds or higher depths. Worthy mentioning is that several authors have proposed different coefficient values, and a more inclusive range is in the order of 0.5−1.0 (Genç et al., 2015; Stumpf et al., 2016; Welber et al., 2016). According to ISO 748:2007 (2007), the entropy parameter M can also be parametrized as a function of the Chézy number on each vertical, leading to a possible parametrisation in function of the Gauckler−Manning−Strickler coefficient as well. Based on these ideas, Bandini et al. (2021) proposed a novel formulation able to simultaneously estimate both the river discharge and Manning's roughness coefficient without the needs for site-specific coefficients (only UAS measurements of surface flow velocities and water surface slope).

9.7.2 Discharge

River discharge can be derived by combining depth-averaged water velocities and cross-sectional area information. If river bed profiles are available, UAS-based image velocimetry data are sufficient for direct discharge estimation (Detert and Weitbrecht, 2016). If this information is not available, water level can be retrieved either from images acquired

by traditional field campaigns and ultrasonic sensors, or following a fully visual framework. The latter is made up of two steps: (1) a pixel-wise segmentation of the current image is used to generate a binary mask separating water and nonwater regions, (2) the mask is analyzed to infer the waterline's position. Using the stabilised image sequence, water lines are detectable, assuming that moving water results in significant changes in the spatio-temporal pixel texture (Kröhnert and Meichsner, 2017). High-resolution data allow the 3D reconstruction of a river scene (a 3D point cloud, digital elevation model) using computer vision techniques (structure from motion). Water stages will be reconstructed, integrating the waterline identified by segmentation approaches with the 3D model (Eltner et al., 2021). This methodology has been recently applied to extrapolate river bathymetry in clear and shallow waters, correcting the refraction effect's underwater areas (Dietrich, 2017). Another UAS-based approach was presented by Bandini et al. (2018), showing the possibility to use sonar technology to measure bathymetry and controlled by a drone. River discharge estimates computed with these innovative methods are in good agreement with standard measurements, typically presenting errors less than 20%–30% (Bandini et al., 2021; Kim et al., 2008; Kinzel and Legleiter, 2019; Le Coz et al., 2010; Lewis and Rhoads, 2018).

9.7.3 Flow patterns

Flow patterns comprise magnitudes and directions of velocity vectors in the study area and may vary depending on the resolution of the velocity field. 2D surface flow patterns are described by the corresponding SVF. They can be validated by means of comparison with surface velocities measured in selected locations of the study area, if these velocities are characterized by both magnitude and direction. A practical example of such comparison can be found in the work of Strelnikova et al. (2020). 3D flow patterns are the result of complex hydrological modeling with the use of either the bathymetry data in the study area and surface SVFs, or depth-average velocities along cross-sections, or flow velocities measured in certain points of the study area. It is not possible to validate the accuracy of calculated flow patterns based solely on discharge reference data or on reference velocity magnitudes.

9.8 Limitations of image velocimetry methods and future perspectives

Even though image-velocimetry techniques are widely used, their accuracy under field conditions is still an issue of research. A common challenge is the influence of environmental noise on the velocity signal. Poor illumination, sunlight reflections, glare and shadows on the flow surface, river color background, riverine flora movements, and apparent ground motion due to instability of a camera represent common sources of environmental noise (Le Coz et al., 2010). These noisy signals can significantly affect image velocimetry results. For instance, stabilization issues or neglected—or poorly executed—camera calibration during field measurement could potentially induce significant errors in a frame-by-frame displacement calculation (Detert, 2021; Ljubičić et al., 2021). Extremely scarce illumination or rapid

illumination changes may introduce several problems in recovering long and reliable trajectories (Pearce et al., 2020; Tauro et al., 2018). Such limitations can be partially compensated using high-visibility tracers or thermal sensors that are less affected by water surface reflections and illumination conditions than RGB imagery. Thermal sensors allow to monitor in daylight and night-time conditions (Fujita, 2017) but their current resolution and price present a limitation for the monitoring of larger rivers or when high level of detail is required. A greater effort is necessary to identify a set of strategies for automatic discrimination of tracking features from water reflections and environmental noise in natural settings and to remove image distortions before image processing (Detert, 2021).

The lack of surface tracking features or distributed materials across the cross-section is still a challenge. Most of the literature experiments were artificially seeded to simplify the identification of moving patterns on the water surface (Perks et al., 2020). In natural conditions, flows are often characterized by low seeding densities or locally distributed tracers and irregular tracer clusters. These conditions can introduce a high variance and underestimate the flow velocity field, especially near the river banks. In this regard, automated deployment and novel environment-friendly materials may be explored to improve the tracers' spatial distribution and reduce the material's tendency to form agglomerates.

A considerable limitation affecting optical methods is also the lack of information on the velocity profile along the vertical. Even if some proof-of-concept experiments have been conducted to demonstrate discharge estimation from image-based methods (Bandini et al., 2021; Detert et al., 2017; Pizarro et al., 2020b), the integration of these methodologies for the estimation of mean velocity in open channels is still an open research question.

In brief, considerable work is needed for establishing standard protocols and guidelines for the implementation of image velocimetry in different settings (flow regimes and illumination conditions). This can allow the selection of image velocimetry methods and procedures for appropriately monitoring stream flows based on morphological field characteristics, environmental factor, and hydraulic conditions.

9.9 Hands-on experience

9.9.1 Site description

In this section, we explore the optimization of the analysis workflow using KLT-IV v1.01 and an example of UAS footage acquired on the River Arrow, United Kingdom. The location of image acquisition is a meandering section of the Arrow River with an approximate width of 5 m. Water depth is shallow (mean = 0.22 m) and water clarity is high, resulting in the river bed being clearly visible. A more detailed characterization of the field site is presented in Perks et al. (2020). A 4 min 14 s video recorded at a frame rate of 29.97 Hz and pixel resolution of 1920×1080 was acquired using a DJI Phantom 4 Pro UAS. During this time the platform hovered over the center of the channel at a height of 12.06 m with the camera oriented at nadir. However, calculations later revealed a camera angle of 4.1 degrees from the vertical. While the UAS operator did not provide any input into the controller, the UAS position did drift during recording. Based on these characteristics, we can identify that a processing workflow would require image stabilization and

orthorectification (see Section 9.4.2). We may also choose to perform image enhancement on the orthophotos to improve detection and tracking of tracers (Section 9.4.3). The required inputs and settings for performing the analysis using KLT are provided in the supplementary information.

9.9.2 Workflow description

Within KLT-IV (Fig. 9.5), we first need to define the video input settings. As we are working on a single video, we can select single video as the mode of analysis, prior to defining the location on the PC of the video to be analyzed. Upon selection, the user will be asked whether reencoding is required. This is only required if the metadata of the video has become corrupted and is not required in this case. Next, we can choose the camera type that is being used. As the DJI Phantom 4 Pro is listed, we can select this camera type. This ensures that lens distortion is explicitly accounted for in the orthorectification process. There are two approaches that could be used for the analysis of this footage: (1) dynamic: GCPs: this approach tracks the location of GCPs and uses this information to stabilize and orthorectify the imagery in one step; alternatively, (2) dynamic: GCPs + stabilization: this approach first utilizes immobile areas within the FOV to stabilize the imagery and then generates orthophotos using GCP data and the stabilised image sequence. For the purposes of this example, we will first stabilize the imagery and then orthorectify using the dynamic: GCPs + stabilization approach. The presence of stable bankside features within the image frame enables an accurate stabilization of the image sequence, rather than relying on the relatively scarce GCPs. This option is selected in the Orientation menu. Now the approximate location of the UAS needs to be provided (in the same coordinate system as the GCPs). Ensuring that the tick box is enabled for each of these parameters will ensure that this location is optimized using the GCP data. The camera pose (view direction) also needs to be provided. The first and third values can

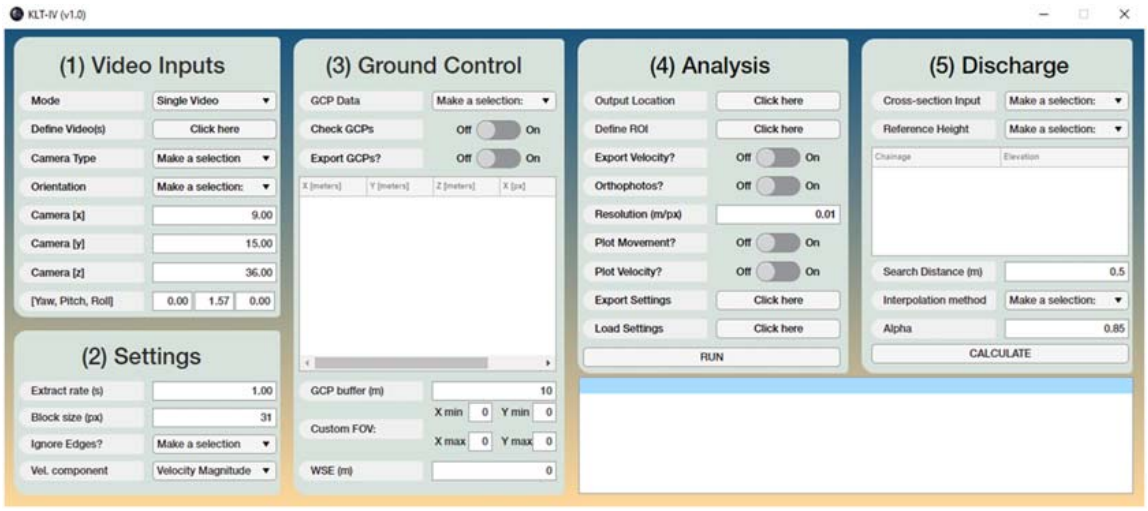

FIGURE 9.5 The graphical user interface of KLT-IV.

be left as zero; however, the pitch value should be approximated. If looking at nadir (vertically down), this value should be 1.57 and for each degree of inclination, 0.017 should be subtracted from this value.

In the settings section, we can identify the duration that features are tracked for before their velocities are computed. Generally, the longer this period is, the more accurately the flow vectors are reconstructed. However, with longer sampling times, the tracers travel over a longer distance and in locations with complex morphology and nonuniform flow patterns (e.g., pool-riffle sequences), this may result in spatial variability being averaged. Generally, a time of between 0.5 and 2 s will suffice. The block size defines the parameter used for searching for detected features. The default value is usually appropriate. Finally, either the velocity magnitude (velocity independent of direction) or the normal component (magnitude along a defined flowline) can be selected. In this case study, the latter is chosen and the user is prompted to define the flowline from upstream to downstream.

We next need to provide ground control information. This can be achieved by selecting each individual GCP on the image and providing the location information, or alternatively importing the data from .csv file with this information provided in the appropriate format (see supplementary information under https://www.costharmonious.eu/). The GCP data can also be exported as a .csv file. By enabling this option, this eliminates the need to select GCPs from the imagery more than once. As part of the analysis process orthophotos may be generated. The user may define the spatial extent of these orthophotos as they see fit. Generally, if GCPs are present on both banks and across the area of interest, then a GCP buffer of zero can be assigned. However, this value can be increased to incorporate a larger area into the orthophotos. Alternatively, a custom FOV can be chosen which explicitly defines the extent of the orthophotos. Finally, the water surface elevation is required. This is in the same coordinate reference system as the GCPs.

The final step is defining the analysis parameters. We first define the output location where all the generated files are stored. Next, we need to define the ROI. The user is required to draw a polygon of the area of interest on an image. Areas within the ROI will be analyzed for movement. When the dynamic: GCPs + stabilization orientation is selected, areas outside of the ROI polygon will be used in the stabilization process. Therefore, when this method is selected, it is important that the defined ROI covers the entire image where movement occurs (even if it is not in the river). Next, the user can identify whether any preprocessing (image enhancement) should be undertaken on the orthorectified imagery. The user can also identify the required outputs. Velocity is exported as a .csv file, orthophotos as a .jpeg at the defined resolution, and velocity vectors can be plotted and automatically exported as a .png. Upon hitting the analysis button, the stabilization and orthorectification process will begin and the user will be asked which portion of the footage should be analyzed. Given the presence of high density of tracers toward the latter parts of the footage, we choose to analyze the video portion spanning 173 and 218-s. This provides 45-s of relatively stable footage with a high density of tracer material present. If image enhancement has been selected, then the user will be prompted with a range of options prior to analysis being undertaken. For the purposes of this example, we run three simulations with different image enhancement procedures to illustrate their effects: (1) no image enhancement; (2) high-pass filter (30 pixels), followed by a wiener filter (8 pixels), and (3) background subtraction followed by high-pass filter (30 pixels) and a Wiener filter (8 pixels).

9.9.3 Appraisal of the outputs

Reference velocity data were acquired through the deployment of a Valeport 801 electromagnetic current meter. Measurements were made for a period of 30-s just below the water surface, with the time-averaged value being reported. Measurements were obtained for five cross-sections spaced approximately 1.5–2 m apart, within which 9–10 individual measurements were obtained with a spacing of 0.5 m between each (Fig. 9.6A). The velocity measurements ranged from 0.07 to 0.62 m/s with an average and standard deviation of 0.42 and 0.10 m/s, respectively. As these reference measurements were made just below the water surface, the image-based measurements and current meter measurements may not be directly comparable but should be closely related. Fig. 9.6B, C, and D present the magnitude and direction of 100,000 successfully tracked tracers. For each example the direction and magnitudes appear to be visually similar, with the fastest flows toward the inner bank in the upper right quadrant of the orthorectified image.

Summary statistics for each of the simulations are provided in Table 9.5. From this information, we can see that the range of the no image enhancement condition without

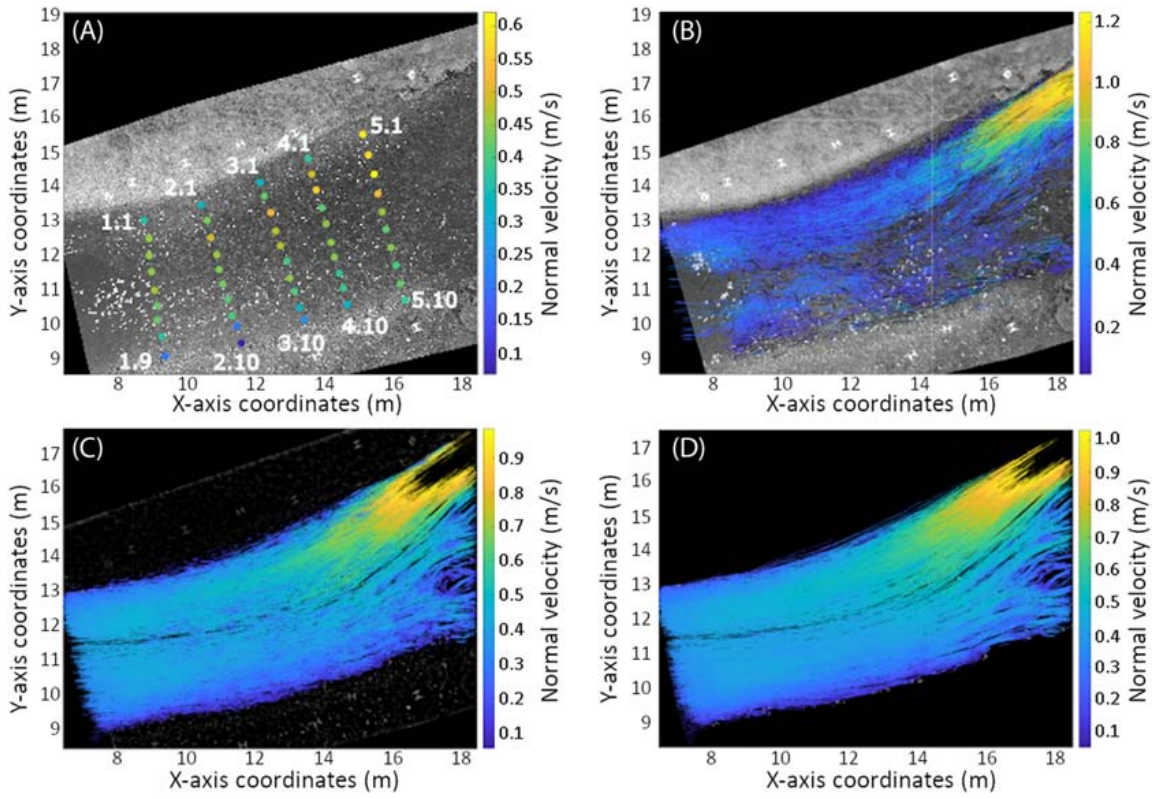

FIGURE 9.6 The location and magnitude of reference velocity measurements (A) in addition to the surface trajectories reconstructed by KLT-IV using (B) the original footage without preprocessing, (C) image sequences exposed to high-pass filter + Wiener filter, and (D) image sequences exposed to background subtraction high-pass filter + Wiener filter. The direction of flow in these images is from left to right.

threshold has an almost identical upper range to that of the reference measurements. However, negative velocities are apparent indicating reconstruction of flow in an upstream direction. Furthermore, the mean velocity is considerably lower than the reference (0.10 vs 0.42 m/s) indicating a considerable bias toward low velocities. When a 0.05 m/s threshold is applied on this no enhancement scenario, the range becomes almost identical to the reference measurements and the mean increases because of the filtering of some very low flow velocities. However, the mean is still biased low relative to the reference (0.21 vs 0.42 m/s). Upon the application of image preprocessing filters, the summary statistics of the outputs improve. With the application of high-pass filter + Wiener filter, the mean flow velocity increases to 0.38 and 0.39 m/s in the with and without thresholds conditions. Furthermore, when background subtraction is applied before the high-pass filter + Wiener filter, the mean becomes almost identical to that of the reference value (0.43 vs 0.42 m/s). When preprocessing procedures are employed to enhance the visibility of tracers or reduce the visibility of the river bed, the results indicate that the impact of post-processing procedures becomes less relevant with the application of a threshold condition having limited effect on the results.

When the outputs of all the configurations are plotted (Fig. 9.7), the impacts of both preprocessing (image enhancement) and postprocessing (filtering) on the results are clear. The configurations with no image enhancement produce velocity estimates that are consistently biased low relative to the reference measurements. This is likely a consequence of the river bed being visible, resulting in higher levels of noise. Upon the application of the high-pass and wiener filters, the velocity estimates are in good agreement with the reference measurements across much of the area. Generally, where these estimates deviate from the reference, they tend to also be biased low, except for xs4. This is again due to the enhancement failing to remove the visible river bed. Only when the image background is subtracted do we see this low bias being removed. With this configuration the velocities are in very good agreement with the reference except for the very edges of the channel where flow depths are very low, and in xs4 and 5 where flow velocities appear to be slightly overestimated.

TABLE 9.5 Summary statistics of the reference velocity measurements and those computed using KLT-IV v1.01 at the same locations.

		Range [m/s]	Mean [m/s]	Standard deviation [m/s]
Reference measurements		0.07–0.62	0.42	0.10
No image enhancement	(Without threshold)	−0.29 to 0.60	0.10	0.14
	(with threshold)	0.07–0.63	0.21	0.13
High-pass filter + Wiener filter	(Without threshold)	0.005–0.81	0.38	0.16
	(with threshold)	0.06–0.81	0.39	0.16
Background subtraction + high-pass filter + Wiener filter	(Without threshold)	0.003–0.81	0.43	0.15
	(with threshold)	0.08–0.81	0.43	0.15

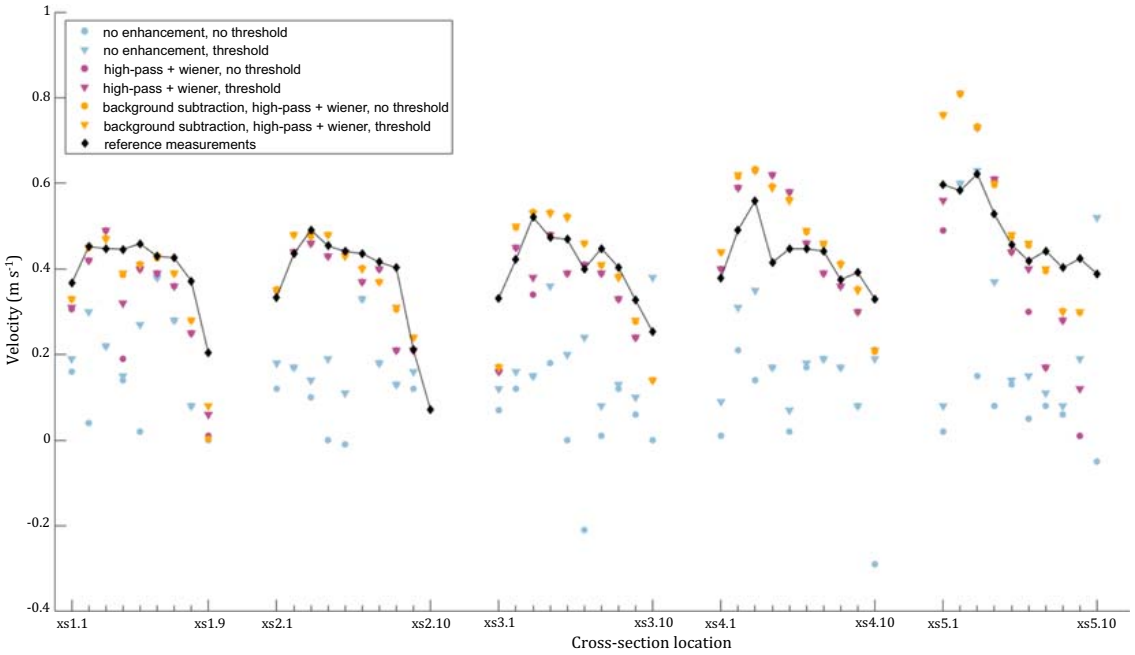

FIGURE 9.7 A comparison between the reference velocities and those generated using KLT-IV v1.01 using a range of pre- and postprocessing solutions. Cross-section transects labeled xs1 to xs5 go from left to right of the image in Fig. 9.6A, and the measurement numbers within each cross-section increase from top to bottom (e.g., 1.1–1.9).

Appendix A Table A1

TABLE A1 Goals, operational principles, and limitations of contact flow measurement methods.

No.	Method	Measured value	Operating principle	Peculiarities and limitations
1	Volumetric streamflow method	Discharge	The flow is directed into a large container of known volume, which must be repeatedly filled with water. In each iteration the time needed to fill the container is recorded. Discharge as calculated as a ratio between the container volume and the time needed to fill it (Gore and Banning, 2017).	Can be applied at narrow streams with the entire flow converging into a single descend (Hauer and Lamberti, 2007).

(*Continued*)

TABLE A1 (Continued)

No.	Method	Measured value	Operating principle	Peculiarities and limitations
2	Flume method	Discharge	A precalibrated channel-type structure is installed into a stream. The discharge can be found in the accompanying table based on water depth.	Suitable for narrow streams. Not suitable for steep slopes. Flume installation is laborious (Dobriyal et al., 2017).
3	Weir method	Discharge	A dam-like structure of standard configuration is installed in a cross-section of the narrow stream. The discharge value is obtained directly from the flow depth based on the chart or table calculated for the given weir configuration. A nonstandard weir requires individual calibration.	Suitable for narrow streams. Intrusive and is likely to negatively influence aquatic species (Carpenter-Bundhoo et al., 2020; Mueller et al., 2011). The correct size of the weir has to be selected based on the discharge range in the target cross-section.
4	Float method	Surface flow velocity	The time it takes a floating object to reach the downstream target line is measured repeatedly and averaged.	Only suitable for straight watercourses with regular flow. In these conditions, it provides results in a high level of agreement with the current meter measurements (Kanu, 2020).
5	Colored dye tracing method	Flow velocity	A strongly colored dye is quickly added to the stream to form a cloud. Its dispersion takes place in all three directions. The time it takes the cloud to travel to the measuring line is recorded. The measurement is repeated several times and averaged.	Dyes may be toxic or form toxic substances when mixed with streamwater (Kilpatrick and Wilson, 1989); thus special attention must be paid to selecting a safe dye. The method is not applicable in turbulent streams.
6	Propeller current meter	Flow velocity	Current meters measure flow velocity directly, by counting the number of propeller rotations per time interval. To measure discharge, multiple measurements are performed with the current meter along a selected cross-section. Water depth is measured in each of the points together with flow velocity. Discharge between the measurement points is calculated as a product of the subsection area and the flow velocity in this subsection.	May deliver wrong values in complicated flows. Applicability in flood conditions is very limited. Not suitable for watercourses with high debris load.

(*Continued*)

TABLE A1 (Continued)

No.	Method	Measured value	Operating principle	Peculiarities and limitations
7	ADCP	Flow velocity	ADCP is mounted to a boat or other vessel moving perpendicular to the flow direction. It transmits acoustic impulses at a constant frequency along several beams. Frequency shifts between impulses and their echoes are used to compute water velocity component for each beam. These components are used to calculate a 3D velocity using trigonometric relations (Yorke and Oberg, 2002).	Suitable for large rivers under varying flow conditions (Yorke and Oberg, 2002). Not optimal in watercourses with dense vegetation (Bialik et al., 2014).
8	Radar surface velocity measurements	Surface flow velocity	This technique is based on using the Doppler effect of radio signal emitted by an antenna and backscattered by short surface waves generated by turbulence, rain or wind (Costa et al., 2006). The surface velocity can be translated into depth-average velocity and discharge information using stage/velocity-discharge relationships. Different portable, permanent, and UAS radars have been deployed in rivers for delivering real-time and continuous time series of velocity and discharge (Fulton et al., 2020).	Although some limitations in very smooth channels and near the river banks, the method results particularly suitable for discharge estimation under high flow conditions where other methodologies fail.
9	Electromagnetic measurements		The method relies on Faraday's law of electromagnetic induction. An electromagnetic flow meter induces a magnetic field. Water flow through this magnetic field produces a difference in electrical potential, which is proportional to flow velocity (Bialik et al., 2014).	Not optimal in watercourses with dense vegetation (Bialik et al., 2014).
10	Dilution gauging	Flow velocity	A tracer solution (often NaCl) is added into a stream at a selected rate and gets uniformly mixed. At a downstream measurement point, electrical conductivity sensor is used to monitor the transport of this solution. The modal flow velocity is defined by the time it takes the tracer solution to achieve the peak concentration at the measurement point (Moore, 2004).	Works well in vegetated (Plew and Hoyle, 2017) and turbulent (Bolognesi et al., 2006) streams. Well suited for small watercourses in all conditions, including very low flow or flood (Tazioli, 2011).

ADCP, Acoustic Doppler current profiler.

Appendix B Data acquisition log

General					
Task ID	Date	Location	Coordinates: x/y	Ref. system	Coordinator
Conditions				Other conditions	
Water color	Turbidity	Water level	Discharge		
Wind	Air temperature	River width	River depth		
UAS and camera					
UAS make	UAS initial X	UAS initial Y	UAS initial height	Gimbal Y/N	D-RTK Y/N
Sensor model	Camera lens	Sensor type	Image resolution	Frame rate	Data format
Data acquisition description					
Tracer		GCPs			
Tracer type, color	Tracer input point	GCP description	GCP coords	GCP description	GCP coords
Start time	End time	Comment			
Reference measurements					
Measurement method/tool		Duration of measurement	Number of measurements	Measurement depth	Direction available Y/N

GCP, Ground control point.

References

Acreman, M.C., Dunbar, M.J., 2004. Defining environmental river flow requirements – a review. Hydrol. Earth Syst. Sci. 8, 861–876. Available from: https://doi.org/10.5194/hess-8-861-2004.

Bandini, F., Olesen, D., Jakobsen, J., Kittel, C.M.M., Wang, S., Garcia, M., et al., 2018. Technical note: bathymetry observations of inland water bodies using a tethered single-beam sonar controlled by an unmanned aerial vehicle. Hydrol. Earth Syst. Sci. 22, 4165–4181. Available from: https://doi.org/10.5194/hess-22-4165-2018.

Bandini, F., Lüthi, B., Peña-Haro, S., Borst, C., Liu, J., Karagkiolidou, S., et al., 2021. A drone-borne method to jointly estimate discharge and manning's roughness of natural streams. Water Resour. Res. 57, 1. Available from: https://doi.org/10.1029/2020WR028266.

Bialik, R., Karpinski, M., Rajwa, A., 2014. Discharge measurements in lowland rivers: field comparison between an electromagnetic open channel flow meter (EOCFM) and an acoustic Doppler current profiler (ADCP). In: Bialik, R., Majdański, M., Moskalik, M. (Eds.), Achievements, History and Challenges in Geophysics. Springer International Publishing, Cham, pp. 213–222.

Bolognesi, A., Gottardi, G., Maglionico, M., 2006. Discharge measurements in a small ungauged river: comparison between conventional current-meter and tracer dilution methods. In: Alves, E., Cardoso, A., Leal, J., Ferreira, R. (Eds.), River Flow 2006. Taylor & Francis.

Brevis, W., Niño, Y., Jirka, G.H., 2011. Integrating cross-correlation and relaxation algorithms for particle tracking velocimetry. Exp. Fluids 50, 135–147. Available from: https://doi.org/10.1007/s00348-010-0907-z.

Cao, L., Weitbrecht, V., Li, D., Detert, M., 2020. Airborne feature matching velocimetry for surface flow measurements in rivers. J. Hydraulic Res. 1–14. Available from: https://doi.org/10.1080/00221686.2020.1818309.

Carpenter-Bundhoo, L., Butler, G.L., Bond, N.R., Bunn, S.E., Reinfelds, I.V., Kennard, M.J., 2020. Effects of a low-head weir on multi-scaled movement and behavior of three riverine fish species. Sci. Rep. 10, 6817. Available from: https://doi.org/10.1038/s41598-020-63005-8.

Chiu, C.-L., 1989. Velocity distribution in open channel flow. J. Hydraulic Eng. 115, 576–594. Available from: https://doi.org/10.1061/(ASCE)0733-9429(1989)115:5(576).

Costa, J.E., Cheng, R.T., Haeni, F.P., Melcher, N., Spicer, K.R., Hayes, E., et al., 2006. Use of radars to monitor stream discharge by noncontact methods. Water Resour. Res. 42, 513. Available from: https://doi.org/10.1029/2005WR004430.

Daigle, A., Bérubé, F., Bergeron, N., Matte, P., 2013. A methodology based on particle image velocimetry for river ice velocity measurement. Cold Reg. Sci. Technol. 89, 36–47. Available from: https://doi.org/10.1016/j.coldregions.2013.01.006.

Dal Sasso, S.F., Pizarro, A., Samela, C., Mita, L., Manfreda, S., 2018. Exploring the optimal experimental setup for surface flow velocity measurements using PTV. Environ. Monit. Assess. 190, 460. Available from: https://doi.org/10.1007/s10661-018-6848-3.

Dal Sasso, S.F., Pizarro, A., Manfreda, S., 2020. Metrics for the quantification of seeding characteristics to enhance image velocimetry performance in rivers. Remote Sens. 12, 1789. Available from: https://doi.org/10.3390/rs12111789.

Detert, M., 2021. How to avoid and correct biased riverine surface image velocimetry. Water Resour. Res. 57, 23 . Available from: https://doi.org/10.1029/2020WR027833.

Detert, M., Weitbrecht, V., 2015. A low-cost airborne velocimetry system: proof of concept. J. Hydraulic Res. 53, 532–539. Available from: https://doi.org/10.1080/00221686.2015.1054322.

Detert, M., Weitbrecht, V., 2016. Estimation of flow discharge by an airborne velocimetry system. La Houille Blanche 33, 13–17. Available from: https://doi.org/10.1051/lhb/2016002.

Detert, M., Johnson, E.D., Weitbrecht, V., 2017. Proof-of-concept for low-cost and non-contact synoptic airborne river flow measurements. Int. J. Remote Sens. 38, 2780–2807. Available from: https://doi.org/10.1080/01431161.2017.1294782.

Dietrich, J.T., 2017. Bathymetric structure-from-motion: extracting shallow stream bathymetry from multi-view stereo photogrammetry. Earth Surf. Process. Landf. 42, 355–364. Available from: https://doi.org/10.1002/esp.4060.

Dobriyal, P., Badola, R., Tuboi, C., Hussain, S.A., 2017. A review of methods for monitoring streamflow for sustainable water resource management. Appl. Water Sci. 7, 2617–2628. Available from: https://doi.org/10.1007/s13201-016-0488-y.

Dugan, J.P., Anderson, S.P., Piotrowski, C.C., Zuckerman, S.B., 2014. Airborne infrared remote sensing of riverine currents. IEEE Trans. Geosci. Remote Sens. 52, 3895–3907. Available from: https://doi.org/10.1109/TGRS.2013.2277815.

Eltner, A., Sardemann, H., Grundmann, J., 2020. Technical note: flow velocity and discharge measurement in rivers using terrestrial and unmanned-aerial-vehicle imagery. Hydrol. Earth Syst. Sci. 24, 1429–1445. Available from: https://doi.org/10.5194/hess-24-1429-2020.

Eltner, A., Bressan, P.O., Akiyama, T., Gonçalves, W.N., Marcato Junior, J., 2021. Using deep learning for automatic water stage measurements. Water Resour. Res. 57, 5. Available from: https://doi.org/10.1029/2020WR027608. 10.

Fujita, I., 2017. Discharge measurements of snowmelt flood by space-time image velocimetry during the night using far-infrared camera. Water 9, 269. Available from: https://doi.org/10.3390/w9040269.

Fujita, I., Hino, T., 2003. Unseeded and seeded PIV measurements of river flows videotaped from a helicopter. J. Vis. 6, 245–252. Available from: https://doi.org/10.1007/BF03181465.

Fujita, I., Kunita, Y., 2011. Application of aerial LSPIV to the 2002 flood of the Yodo River using a helicopter mounted high density video camera. J. Hydro-environment Res. 5, 323–331. Available from: https://doi.org/10.1016/j.jher.2011.05.003.

Fujita, I., Muste, M., Kruger, A., 1998. Large-scale particle image velocimetry for flow analysis in hydraulic engineering applications. J. Hydraulic Res. 36, 397–414. Available from: https://doi.org/10.1080/00221689809498626.

Fujita, I., Watanabe, H., Tsubaki, R., 2007. Development of a non-intrusive and efficient flow monitoring technique: the space-time image velocimetry (STIV). Int. J. River Basin Manag. 5, 105–114. Available from: https://doi.org/10.1080/15715124.2007.9635310.

Fujita, I., Notoya, Y., Shimono, M., 2015. Development of UAV-based river surface velocity measurement by STIV based on high-accurate image stabilization techniques. In: Proc. of the 36th IAHR World Congress, 28 June–3 July, 2015, The Hague, the Netherlands, pp. 6602–6611.

Fujita, I., Notoya, Y., Tani, K., Tateguchi, S., 2019. Efficient and accurate estimation of water surface velocity in STIV. Env. Fluid Mech. 19, 1363–1378. Available from: https://doi.org/10.1007/s10652-018-9651-3.

Fulton, J.W., Anderson, I.E., Chiu, C.-L., Sommer, W., Adams, J.D., Moramarco, T., et al., 2020. QCam: SUAS-based Doppler radar for measuring river discharge. Remote Sens. 12, 3317. Available from: https://doi.org/10.3390/rs12203317.

Genç, O., Ardıçlıoğlu, M., Ağıralioğlu, N., 2015. Calculation of mean velocity and discharge using water surface velocity in small streams. Flow. Meas. Instrum. 41, 115–120. Available from: https://doi.org/10.1016/j.flowmeasinst.2014.10.013.

Gleick, P.H., 2003. Water use. Annu. Rev. Environ. Resour. 28, 275–314. Available from: https://doi.org/10.1146/annurev.energy.28.040202.122849.

Goes, B.J.M., Clark, A.K., Bashar, K., 2021. Water allocation strategies for meeting dry-season water requirements for Ganges Kobadak Irrigation Project in Bangladesh. Int. J. Water Resour. Dev. 37, 300–320. Available from: https://doi.org/10.1080/07900627.2020.1763265.

Gore, J.A., Banning, J., 2017. Discharge Measurements and Streamflow Analysis. Elsevier, pp. 49–70. Available from: https://doi.org/10.1016/b978-0-12–416558-8.00003-2.

Hauer, F.R., Lamberti, G.A., 2007. Methods in Stream Ecology. Academic Press/Elsevier, San Diego, CA.

ISO 748:2007, 2007. Hydrometry—Measurement of Liquid Flow in Open Channels Using Current-Meters or Floats. Retrieved from: <https://www.iso.org/standard/37573.html>.

Jeziorska, J., 2019. UAS for wetland mapping and hydrological modeling. Remote Sens. 11, 1997. Available from: https://doi.org/10.3390/rs11171997.

John, P.H., 1978. Discharge measurement in lower order streams. Int. Rev. ges. Hydrobiol. Hydrogr. 63, 731–755. Available from: https://doi.org/10.1002/iroh.19780630602.

Kanu, I., 2020. Stream Flow Measurement: Development of a Relationship between the Float Method and the Current Meter Method, EGU General Assembly 2020, Online, 4–8 May 2020, EGU2020-21719, https://doi.org/10.5194/egusphere-egu2020-21719.

Kazubek, M., 2003. Wavelet domain image denoising by thresholding and Wiener filtering. IEEE Signal. Process. Lett. 10, 324–326. Available from: https://doi.org/10.1109/LSP.2003.818225.

Kiedrzyńska, E., Kiedrzyński, M., Zalewski, M., 2015. Sustainable floodplain management for flood prevention and water quality improvement. Nat. Hazards 76, 955–977. Available from: https://doi.org/10.1007/s11069-014-1529-1.

Kilpatrick, F.A., Wilson, J.F., 1989. Measurement of Time of Travel in Streams by Dye Tracing. U.S. Government Printing Office, Illinois, USA.

Kim, Y., Muste, M., Hauet, A., Krajewski, W.F., Kruger, A., Bradley, A., 2008. Stream discharge using mobile large-scale particle image velocimetry: a proof of concept. Water Resour. Res. 44, 261. Available from: https://doi.org/10.1029/2006WR005441.

Kinzel, P., Legleiter, C., 2019. sUAS-based remote sensing of river discharge using thermal particle image velocimetry and bathymetric LiDAR. Remote Sens. 11, 2317. Available from: https://doi.org/10.3390/rs11192317.

Koutalakis, P., Tzoraki, O., Zaimes, G., 2019. UAVs for hydrologic scopes: application of a low-cost UAV to estimate surface water velocity by using three different image-based methods. Drones 3, 14. Available from: https://doi.org/10.3390/drones3010014.

Kröhnert, M., Meichsner, R., 2017. Segmentation of environmental time lapse image sequences for the determination of shore lines captured by hand-held smartphone cameras. ISPRS Ann. Photogramm. Remote Sens. Spat. Inf. Sci. IV 2/W4, 1–8. Available from: https://doi.org/10.5194/isprs-annals-IV-2-W4-1-2017.

Le Coz, J., Hauet, A., Pierrefeu, G., Dramais, G., Camenen, B., 2010. Performance of image-based velocimetry (LSPIV) applied to flash-flood discharge measurements in Mediterranean rivers. J. Hydrol. 394, 42–52. Available from: https://doi.org/10.1016/j.jhydrol.2010.05.049.

Le Coz, J., Jodeau, M., Hauet, A., Marchand, B., Le Boursicaud, R., 2014. Image-based velocity and discharge measurements in field and laboratory river engineering studies using the free FUDAA-LSPIV software. In: Proc. of the International Conference on Fluvial Hydraulics (RIVER FLOW 2014). 3–5 September, Lausanne, Switzerland, pp. 1961–1967.

Leitão, J.P., Peña-Haro, S., Lüthi, B., Scheidegger, A., Moy de Vitry, M., 2018. Urban overland runoff velocity measurement with consumer-grade surveillance cameras and surface structure image velocimetry. J. Hydrol. 565, 791–804. Available from: https://doi.org/10.1016/j.jhydrol.2018.09.001.

Lewis, Q.W., Rhoads, B.L., 2018. LSPIV measurements of two-dimensional flow structure in streams using small unmanned aerial systems: 1. Accuracy assessment based on comparison with stationary camera platforms and in-stream velocity measurements. Water Resour. Res. 54, 8000–8018. Available from: https://doi.org/10.1029/2018WR022550.

Ljubičić, R.D., Strelnikova, D., Perks, M.T., Dal Sasso, S.F., Eltner, A., Peña-Haro, S., et al., 2021. A comparison of tools and techniques for stabilising unmanned aerial system (UAS) imagery for surface flow observations. Hydrol. Earth Syst. Sci. 25, 5105–5132. Available from: https://doi.org/10.5194/hess-25-5105-2021.

Manfreda, S., Dal Sasso, S.F., Pizarro, A., Tauro, F., 2019. New insights offered by UAS for river monitoring. In: Sharma, J.B. (Ed.), Applications of Small Unmanned Aircraft Systems, 2019. CRC Press/Taylor & Francis Group, Boca Raton, Florida, pp. 211–234.

Moore, R.D., 2004. Introduction to salt dilution gauging for streamflow measurement part 2: constant-rate injection. Streamline Watershed Manag. Bull. 8, 11–15.

Moramarco, T., Saltalippi, C., Singh, V.P., 2004. Estimation of mean velocity in natural channels based on Chiu's velocity distribution equation. J. Hydrol. Eng. 9, 42–50. Available from: https://doi.org/10.1061/(ASCE)1084-0699(2004)9:1(42).

Mueller, M., Pander, J., Geist, J., 2011. The effects of weirs on structural stream habitat and biological communities. J. Appl. Ecol. 48, 1450–1461. Available from: https://doi.org/10.1111/j.1365-2664.2011.02035.x.

Muste, M., Fujita, I., Hauet, A., 2008. Large-scale particle image velocimetry for measurements in riverine environments. Water Resour. Res. 44, 509. Available from: https://doi.org/10.1029/2008WR006950.

Pearce, S., Ljubičić, R., Peña-Haro, S., Perks, M.T., Tauro, F., Pizarro, A., et al., 2020. An evaluation of image velocimetry techniques under low flow conditions and high seeding densities using unmanned aerial systems. Remote Sens. 12, 232. Available from: https://doi.org/10.3390/rs12020232.

Perks, M.T., 2020. KLT-IV v1.0: image velocimetry software for use with fixed and mobile platforms. Geosci. Model. Dev. 13, 6111–6130. Available from: https://doi.org/10.5194/gmd-13-6111-2020.

Perks, M.T., Russell, A.J., Large, A.R.G., 2016. Technical note: advances in flash flood monitoring using unmanned aerial vehicles (UAVs). Hydrol. Earth Syst. Sci. 20, 4005–4015. Available from: https://doi.org/10.5194/hess-20-4005-2016.

Perks, M.T., Dal Sasso, S.F., Hauet, A., Jamieson, E., Le Coz, J., Pearce, S., et al., 2020. Towards harmonisation of image velocimetry techniques for river surface velocity observations. Earth Syst. Sci. Data 12, 1545–1559. Available from: https://doi.org/10.5194/essd-12-1545-2020.

Pizarro, A., Dal Sasso, S.F., Manfreda, S., 2020a. Refining image-velocimetry performances for streamflow monitoring: seeding metrics to errors minimization. Hydrological Process. 34, 5167–5175. Available from: https://doi.org/10.1002/hyp.13919.

Pizarro, A., Dal Sasso, S.F., Perks, M.T., Manfreda, S., 2020b. Identifying the optimal spatial distribution of tracers for optical sensing of stream surface flow. Hydrol. Earth Syst. Sci. 24, 5173–5185. Available from: https://doi.org/10.5194/hess-24-5173-2020.

Pizer, S.M., Amburn, E.P., Austin, J.D., Cromartie, R., Geselowitz, A., Greer, T., et al., 1987. Adaptive histogram equalization and its variations. Computer Vision, Graphics, Image Process. 39, 355–368. Available from: https://doi.org/10.1016/S0734-189X(87)80186-X.

Plew, D.R., Hoyle, J., 2017. Dilution gauging measurements of discharge in vegetated stream channels. J. Hydrol. (N. Zealand) 56, 31–46.

Pumo, D., Alongi, F., Ciraolo, G., Noto, L.V., 2021. Optical methods for river monitoring: a simulation-based approach to explore optimal experimental setup for LSPIV. Water 13, 247. Available from: https://doi.org/10.3390/w13030247.

Raffel, M., Willert, C.E., Scarano, F., Kähler, C.J., Wereley, S.T., Kompenhans, J., 2018. Particle Image Velocimetry. Springer International Publishing, Cham.

Renzetti, S., 2002. The Economics of Water Demands. Springer, US, Boston, MA.

Samarage, C.R., Carberry, J., Hourigan, K., Fouras, A., 2012. Optimisation of temporal averaging processes in PIV. Exp. Fluids 52, 617–631. Available from: https://doi.org/10.1007/s00348-011-1080-8.

Schoengold, K., Zilberman, D., 2007. The Economics of Water, Irrigation, and Development. Elsevier, 10.1016/s1574-0072(06)03058-1, 2933-2977.

Setiati, N.R., 2019. The feasibility study of bridge construction plan in Digoel River Province of Papua. IOP Conf. Ser.: Earth Environ. Sci. 235, 12083. Available from: https://doi.org/10.1088/1755-1315/235/1/012083.

Shavit, U., Lowe, R.J., Steinbuck, J.V., 2007. Intensity capping: a simple method to improve cross-correlation PIV results. Exp. Fluids 42, 225–240. Available from: https://doi.org/10.1007/s00348-006-0233-7.

Strelnikova, D., Paulus, G., Käfer, S., Anders, K.-H., Mayr, P., Mader, H., et al., 2020. Drone-based optical measurements of heterogeneous surface velocity fields around fish passages at hydropower dams. Remote Sens. 12, 384. Available from: https://doi.org/10.3390/rs12030384.

Stumpf, A., Augereau, E., Delacourt, C., Bonnier, J., 2016. Photogrammetric discharge monitoring of small tropical mountain rivers: a case study at Rivière des Pluies, Réunion Island. Water Resour. Res. 52, 4550–4570. Available from: https://doi.org/10.1002/2015WR018292.

Sukhodolov, A., Uijttewaal, S.W.J., Schnauder, I., Sukhodolova, T., Erdbrink, C., Brevis, W., et al., 2007. Flow visualisation in natural streams: examples and perspectives. In: 32nd Congress of IAHR. 1–6 July Venice, Italy, pp. 68.

Sutarto, T.E., 2015. Application of large scale particle image velocimetry (LSPIV) to identify flow pattern in a Channel. Procedia Eng. 125, 213–219. Available from: https://doi.org/10.1016/j.proeng.2015.11.031.

Tang, H.-w, Chen, C., Chen, H., Huang, J.-t, 2008. An improved PTV system for large-scale physical river model. J. Hydrodyn. 20, 669–678. Available from: https://doi.org/10.1016/S1001-6058(09)60001-9.

Tauro, F., Grimaldi, S., 2017. Ice dices for monitoring stream surface velocity. J. Hydro-environment Res. 14, 143–149. Available from: https://doi.org/10.1016/j.jher.2016.09.001.

Tauro, F., Grimaldi, S., Petroselli, A., Porfiri, M., 2012. Fluorescent particle tracers for surface flow measurements: A proof of concept in a natural stream. Water Resour. Res. 48, 327. Available from: https://doi.org/10.1029/2011WR011610.

Tauro et al. 2014a with the following: Tauro, F., Olivieri, G., Petroselli, A., Porfiri, M., Grimaldi, S., 2014a. Technical note: surface water velocity observations from a camera: a case study on the Tiber river. Hydrol. Earth Syst. Sci. Discuss. 11, 11883–11904. Available from: https://doi.org/10.5194/hessd-11-11883-2014.

Tauro, F., Porfiri, M., Grimaldi, S., 2014b. Orienting the camera and firing lasers to enhance large scale particle image velocimetry for streamflow monitoring. Water Resour. Res. 50, 7470–7483. Available from: https://doi.org/10.1002/2014WR015952.

Tauro, F., Porfiri, M., Grimaldi, S., 2016. Surface flow measurements from drones. J. Hydrol. 540, 240–245. Available from: https://doi.org/10.1016/j.jhydrol.2016.06.012.

Tauro, F., Tosi, F., Mattoccia, S., Toth, E., Piscopia, R., Grimaldi, S., 2018. Optical tracking velocimetry (OTV): leveraging optical flow and trajectory-based filtering for surface streamflow observations. Remote Sens. 10, . Available from: https://doi.org/10.3390/rs101220102010.

Tazioli, A., 2011. Experimental methods for river discharge measurements: comparison among tracers and current meter. Hydrological Sci. J. 56, 1314–1324. Available from: https://doi.org/10.1080/02626667.2011.607822.

Theunissen, R., Scarano, F., Riethmuller, M.L., 2010. Spatially adaptive PIV interrogation based on data ensemble. Exp. Fluids 48, 875–887. Available from: https://doi.org/10.1007/s00348-009-0782-7.

Thielicke, W., Stamhuis, E.J., 2014. PIVlab – towards user-friendly, affordable and accurate digital particle image velocimetry in MATLAB. J. Open. Res. Softw. 2, 1202. Available from: https://doi.org/10.5334/jors.bl.

Welber, M., Le Coz, J., Laronne, J.B., Zolezzi, G., Zamler, D., Dramais, G., et al., 2016. Field assessment of noncontact stream gauging using portable surface velocity radars (SVR). Water Resour. Res. 52, 1108–1126. Available from: https://doi.org/10.1002/2015WR017906.

Westerweel, J., 1994. Efficient detection of spurious vectors in particle image velocimetry data. Exp. Fluids 16-16, 236–247. Available from: https://doi.org/10.1007/BF00206543.

Yorke, T.H., Oberg, K.A., 2002. Measuring river velocity and discharge with acoustic Doppler profilers. Flow. Meas. Instrum. 13, 191–195. Available from: https://doi.org/10.1016/S0955-5986(02)00051-1.

Zeiringer, B., Seliger, C., Greimel, F., Schmutz, S., 2018. River hydrology, flow alteration, and environmental flow. In: Schmutz, S., Sendzimir, J. (Eds.), Riverine Ecosystem Management. Springer International Publishing, Cham, pp. 67–89.